Experimental investigation and numerical modelling of top of rail products

Ing. Daniel Kvarda
Supervisor: **prof. Ing. Martin Hartl, Ph.D.**
Co-supervisor: **Ing. Milan Omasta, Ph.D.**

INSTITUTE OF MACHINE AND INDUSTRIAL DESIGN

BRNO UNIVERSITY OF TECHNOLOGY

CONTENT

Railways as a competitive transport option

Attractive and sustainable way to connect people and businesses

Greenhouse gas emissions from transport (EU-28, 2017)

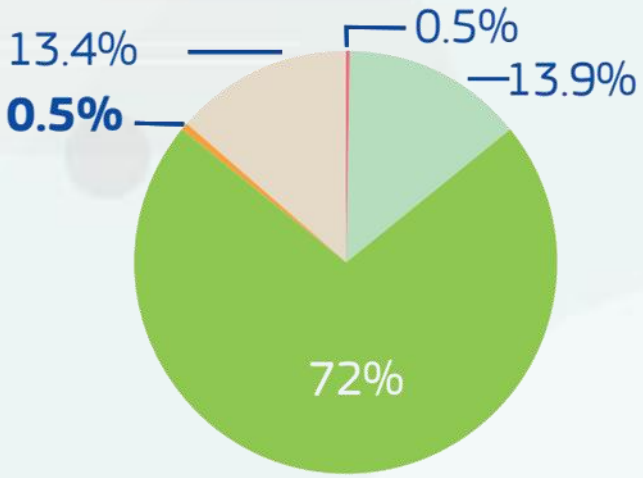

- Road transportation
- **Railways**
- Navigation (including international)
- Other
- Civil aviation (including international)

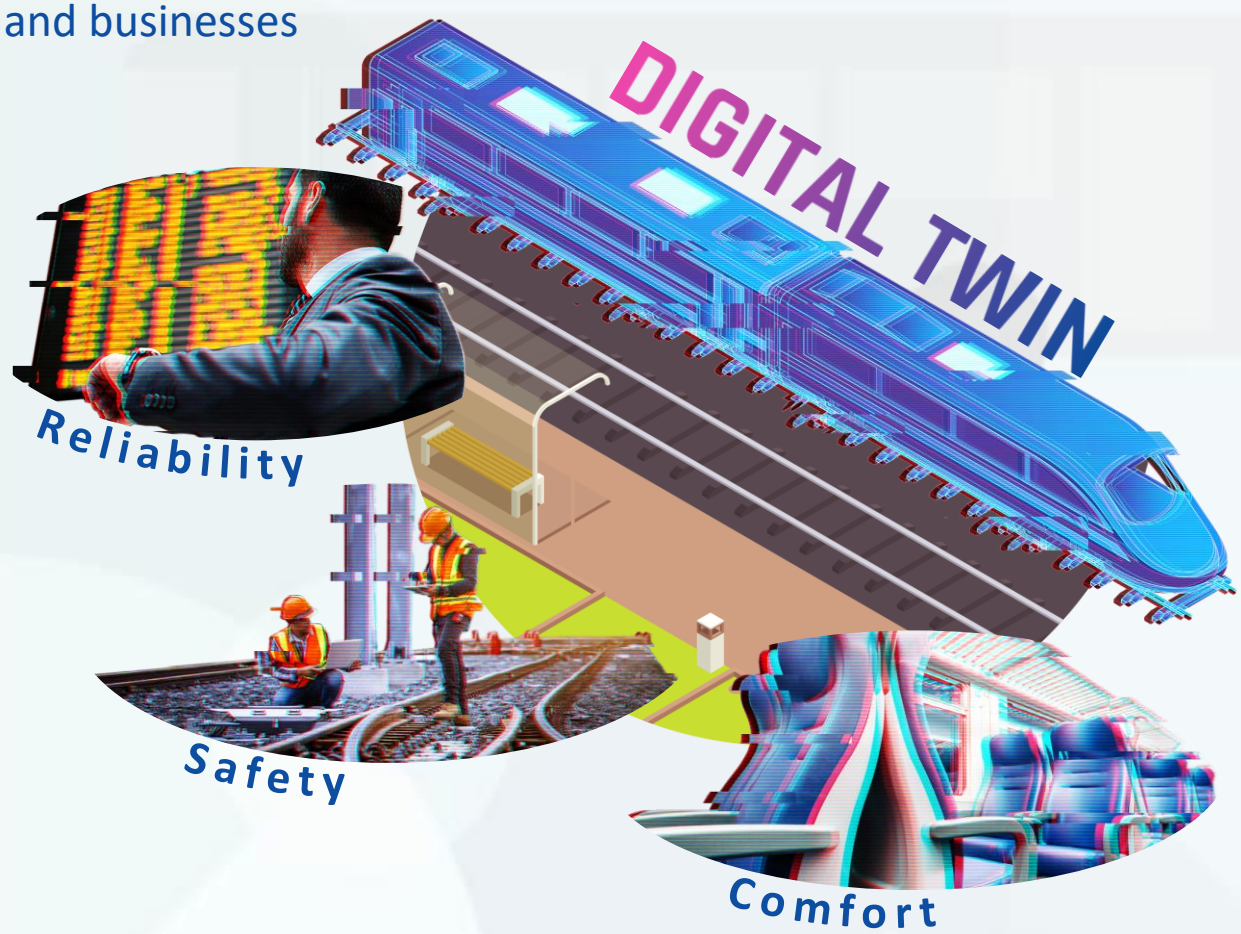

Since 2014, the European Union has allocated more than **EUR 35 billion** to rail

Digitalization in railway transport

Automation

Predictive maintenance

Open data

2021: The European Year of Rail. The European Green Deal.

INTRODUCTION

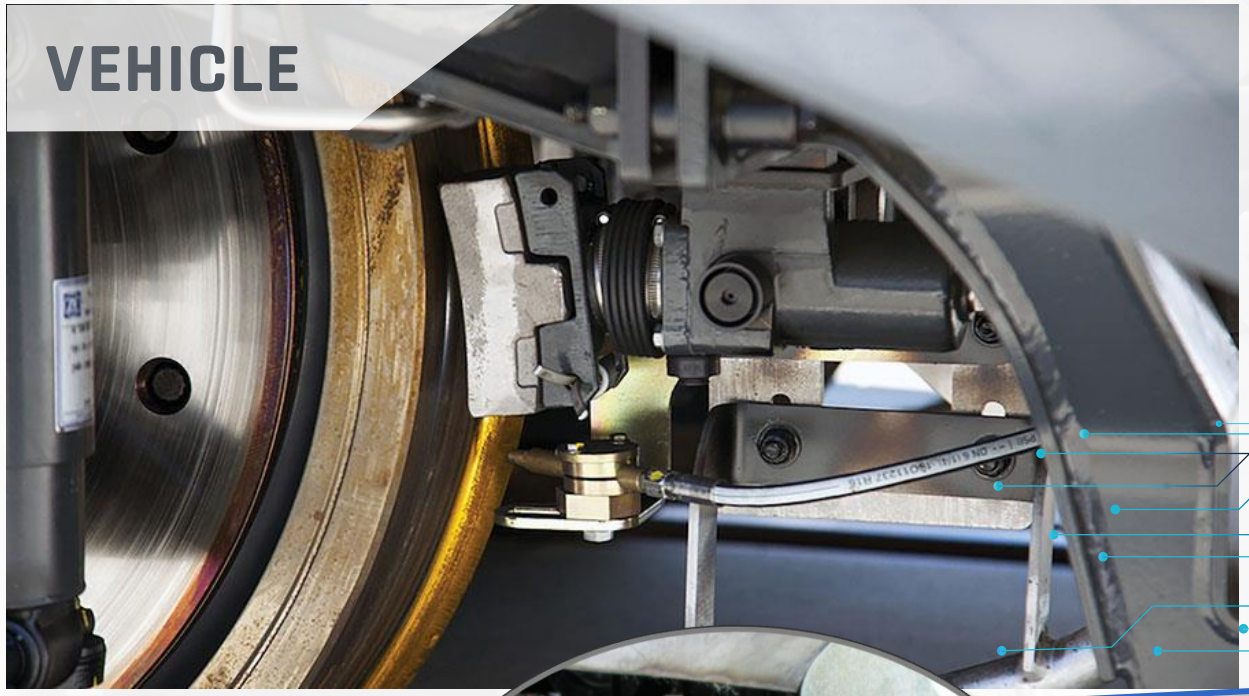

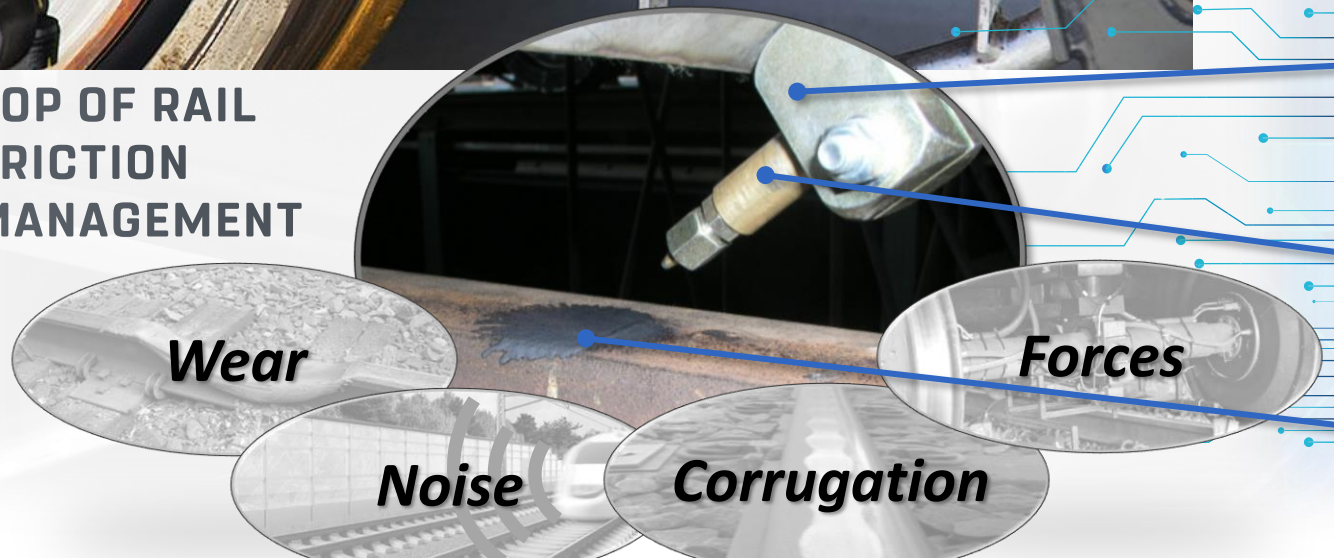

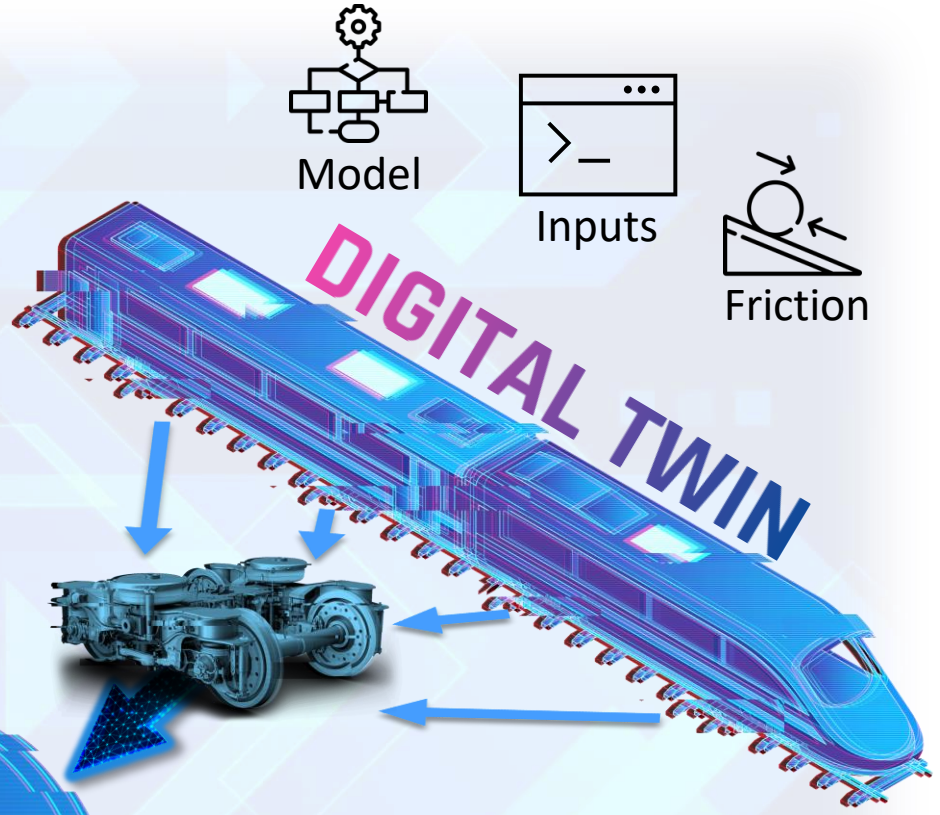

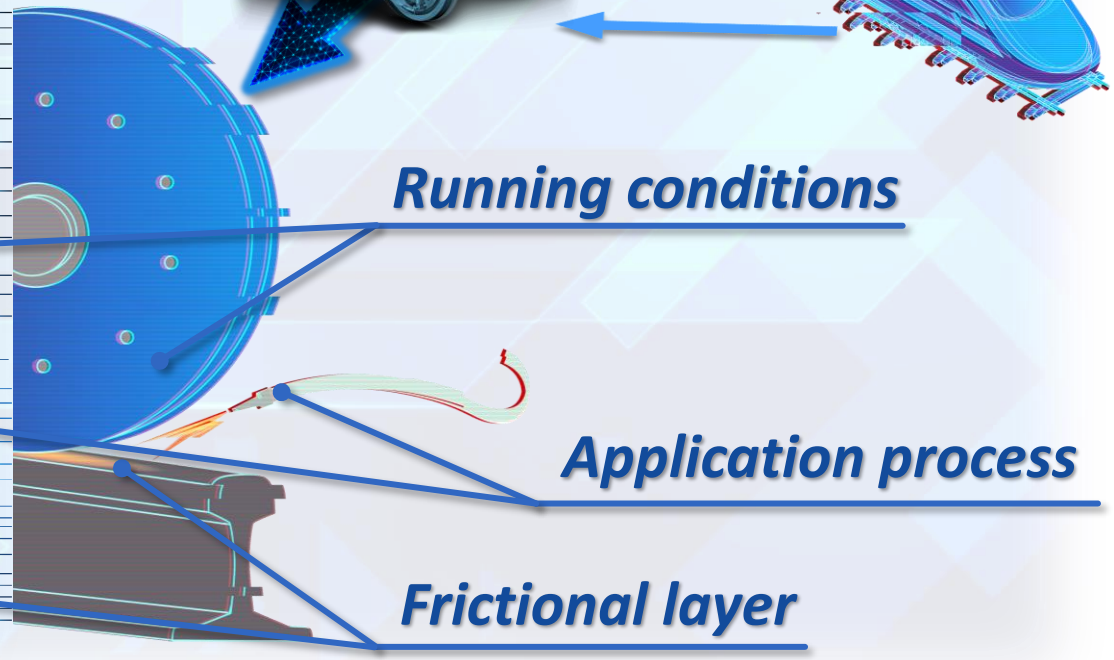

STATE OF THE ART

Top of rail products

Experiment

Frictional properties
Shear properties

Model

Third body layer model
Elastohydrodynamic effect

STATE OF THE ART

Experiment | **Frictional measurements**

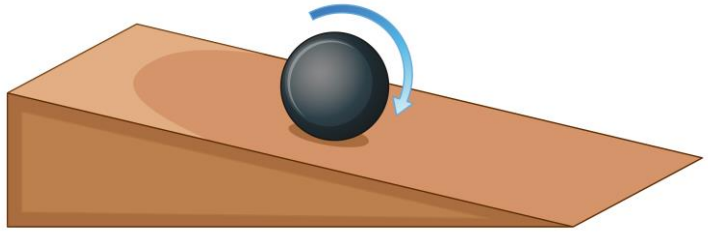

Coefficient of Adhesion

Rolling-sliding

Sliding

Coefficient of friction (Shear stress)

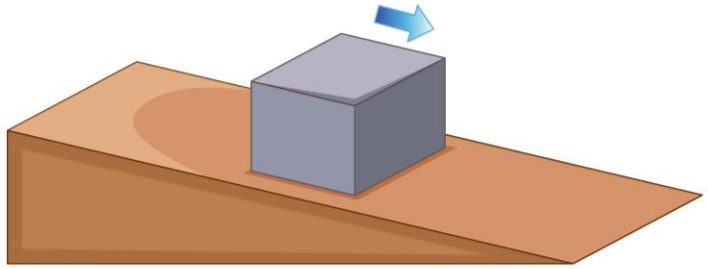

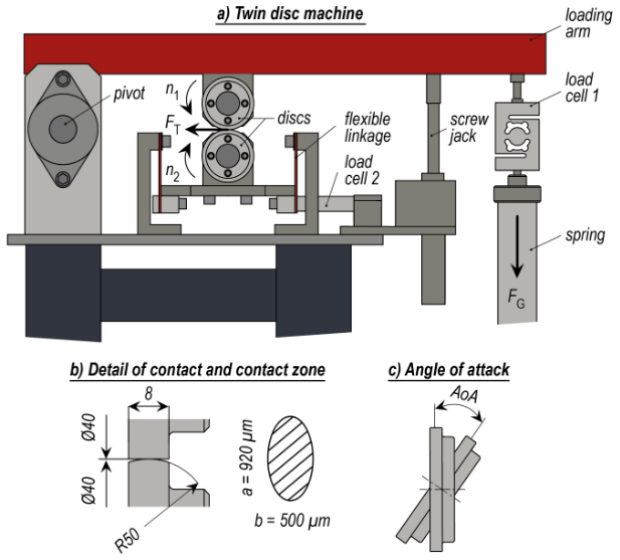

Galas, 2017

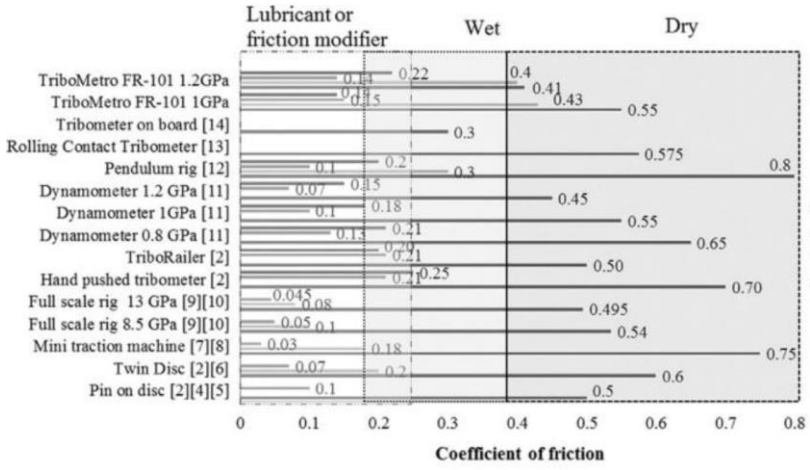

Areiza, 2014

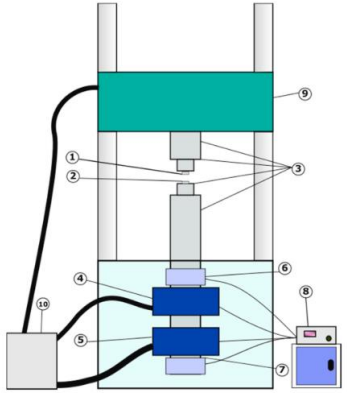

Evans, 2021

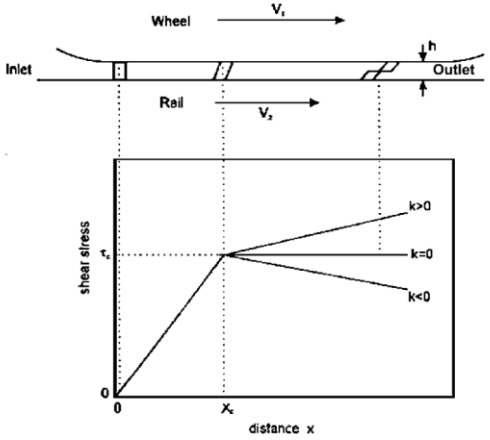

Hou, 1997

STATE OF THE ART

Experiment | **Frictional properties**

- Benefits are linked to two main properties:

Optimal level of friction

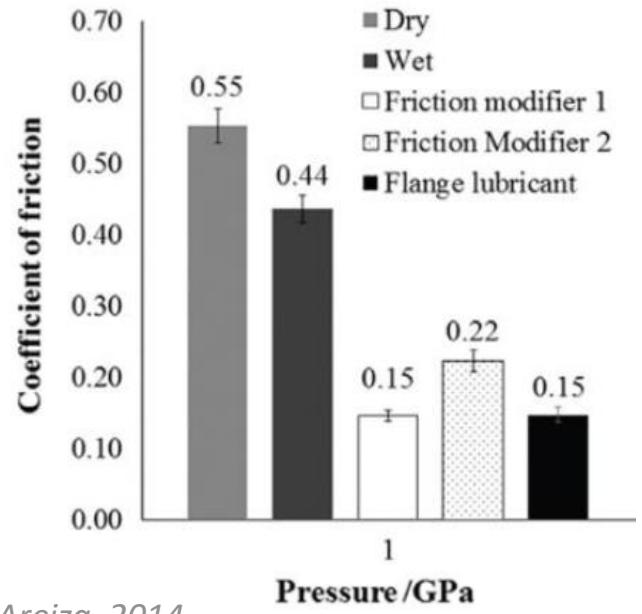

Areiza, 2014

Positive trend of traction curve

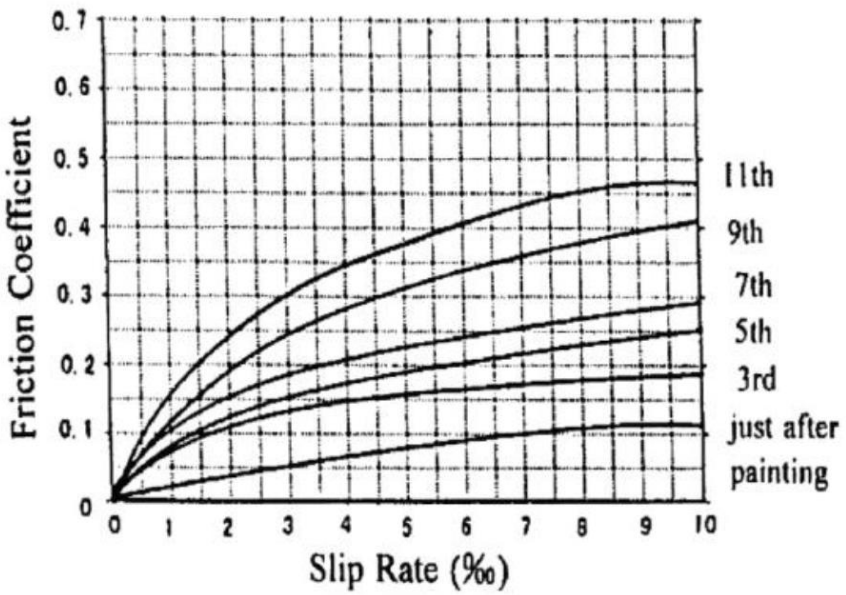

Tomeoka, 2002

Top of rail lubricant

Friction modifier

Solid friction modifier

STATE OF THE ART

Experiment | **Frictional properties**

Top of rail lubricant

- Top of rail lubricants can cause **over-lubrication**.
- Large adhesion drop after application.
- Applied quantity dependent.

Top of rail lubricant

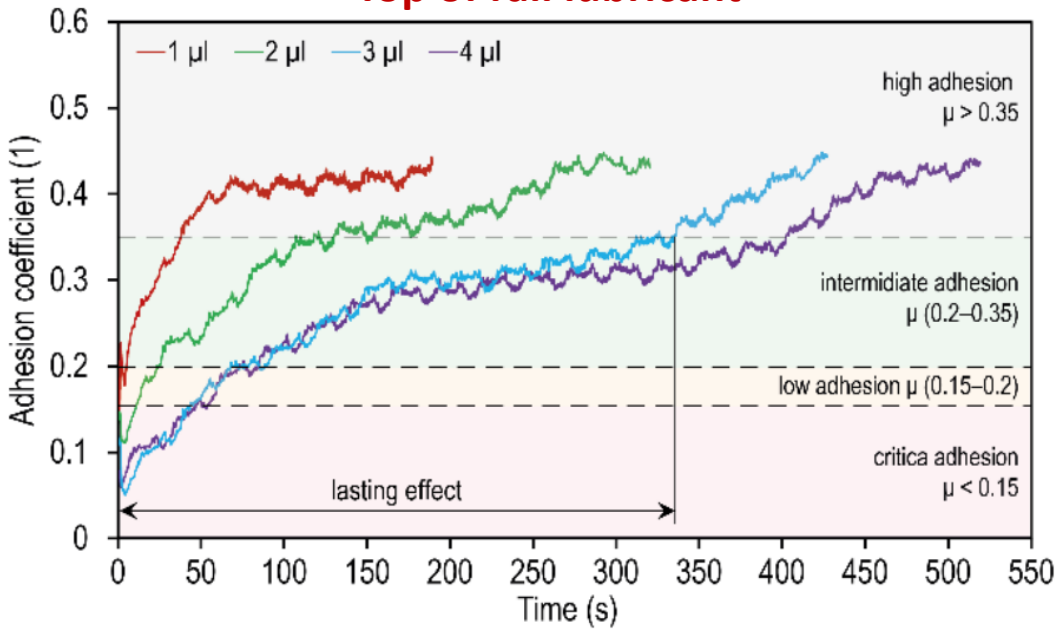

Galas, 2017

Hybrid TORL 

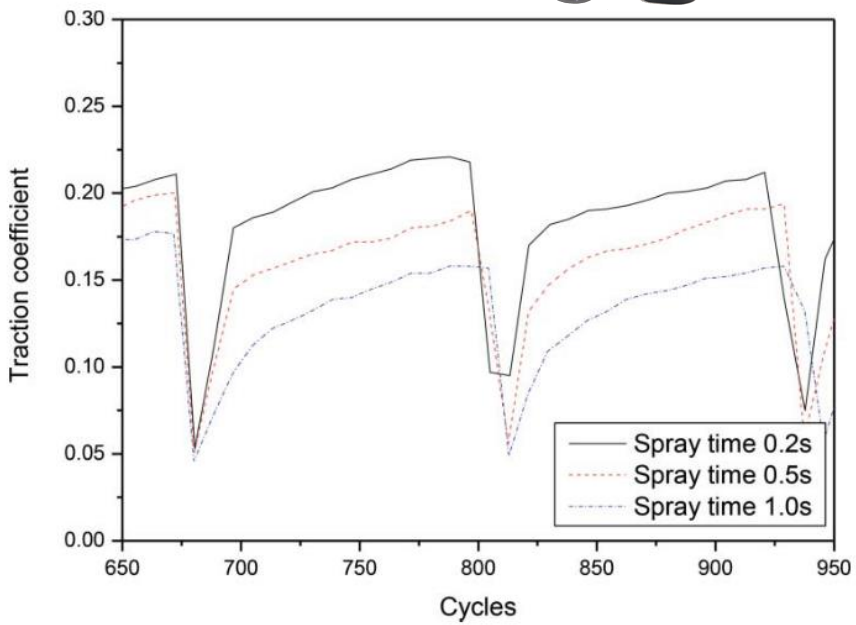

Seo, 2016

STATE OF THE ART

Experiment | **Frictional properties**

- Both *friction modifier* and *solid friction modifier* provide greater resilience to low adhesion after application.
- Friction modifier can be present in both “wet” and “dry” state.
- In “wet” state the *friction modifier* can show decrease in adhesion.

Friction modifier

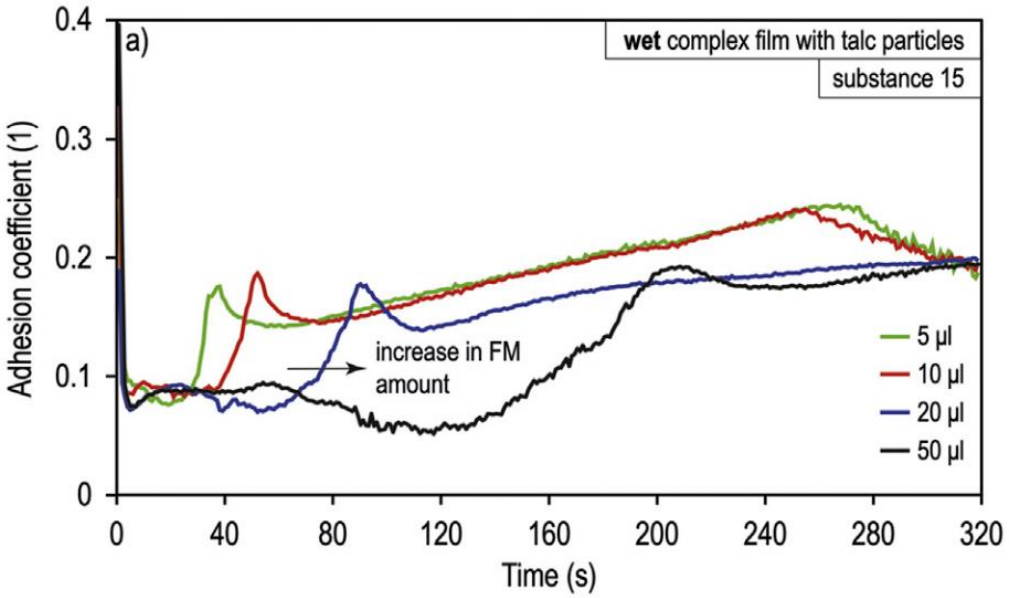

Galas, 2018

Solid friction modifier

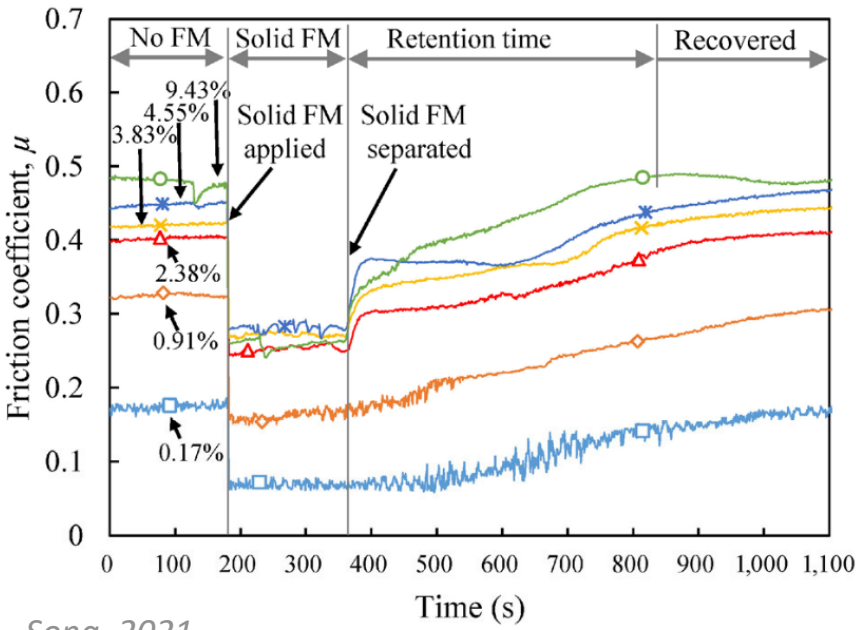

Song, 2021

Friction modifier

Solid friction modifier

STATE OF THE ART

Experiment | **Rheological properties**

- *High pressure torsion* testing
- Shear response to displacement loading
- Elastic and pseudoplastic shearing region
- Identification of **model inputs**

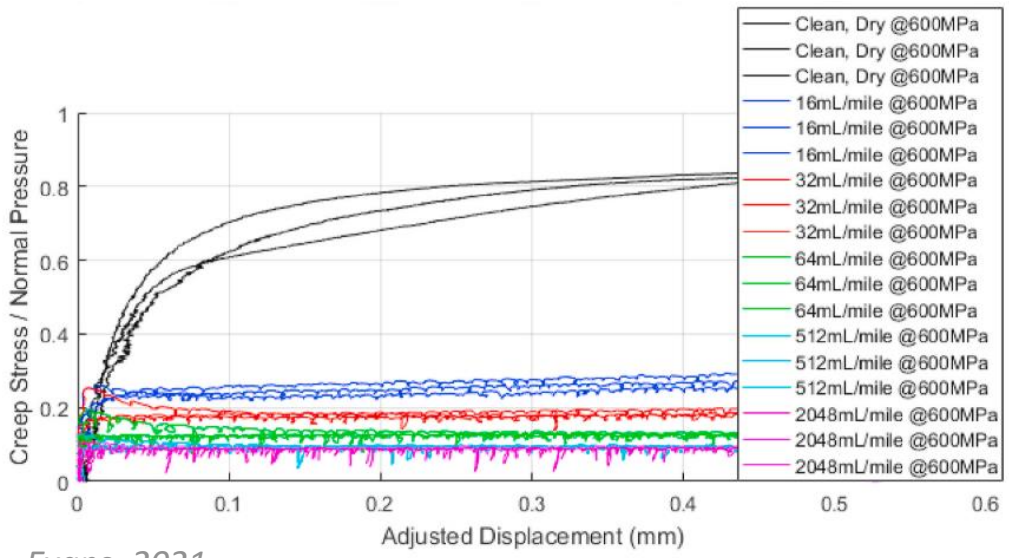

Evans, 2021

Friction modifier

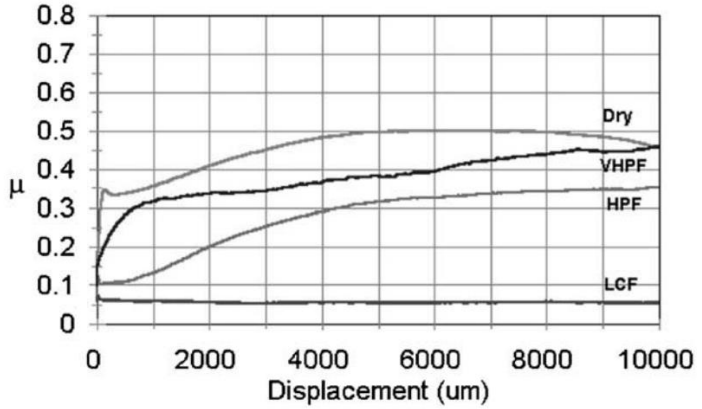

Harrison, 2002

Shearing progression

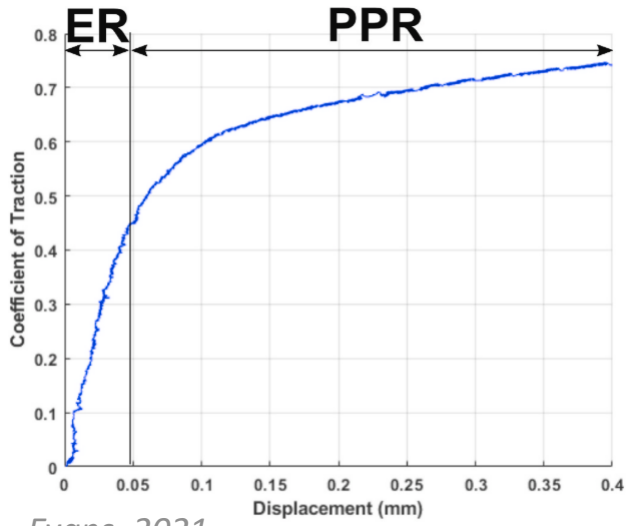

Evans, 2021

Benefits of HPT testing

- Constant contact pressure
- Larger contact area
- Independent of slip rate (%)
- Small sliding distance

STATE OF THE ART

Mathematical model | **Overview of wheel/rail models**

- Exact solution (CONTACT)
  - Benchmark for contact calculations
  - Computationally demanding
- Derived numerical solutions (FASTSIM)
  - Compromise between accuracy/time demands
- Analytical formulas (Kalker's linear theory)
  - Simple implementation with a fast solution

$$F = -\frac{2\mu N}{\pi}\left(\frac{\varepsilon}{1+\varepsilon^2} + \arctan\varepsilon\right)$$

$$\max_{u,p} U = -\int_U \left(h + \frac{1}{2}u_z\right) p\,dU - \int_U \left(w_t + \frac{1}{2}u_t - u_t^*\right)\sigma_t\,dU$$

$$\frac{s_x}{VL} = \frac{\nu_x}{L_1} - \frac{\phi y}{L_3} - \frac{\partial \sigma_{tx}}{\partial x}$$

$$\frac{s_y}{VL} = \frac{\nu_y}{L_2} + \frac{\phi x}{L_3} - \frac{\partial \sigma_{ty}}{\partial x}$$

$$F(F_x, F_y) = \begin{cases} \frac{\mu N}{\tau}\left[(1-|\tau|)^3 \quad \right] & \text{for } |\tau| \geq 3 \\ -\frac{\mu N}{\tau}(\quad) & \end{cases}$$

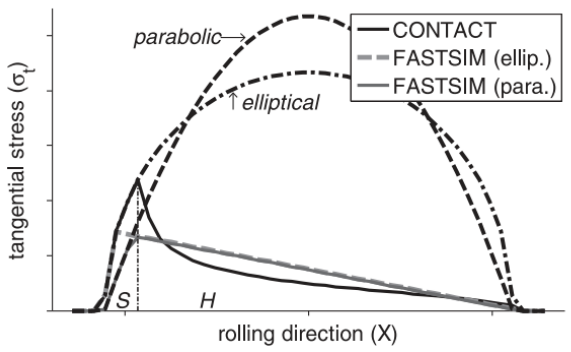

Meymand, 2016

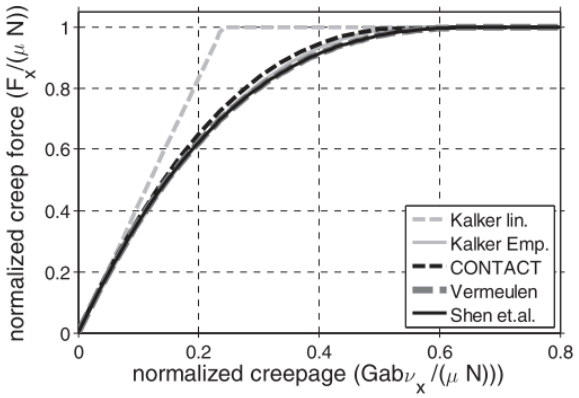

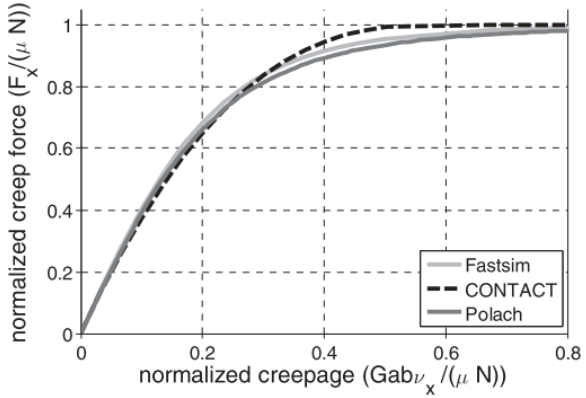

STATE OF THE ART

Mathematical model | **Third body layer**

- Deviation from experimental observations
- Influence of different physical phenomena

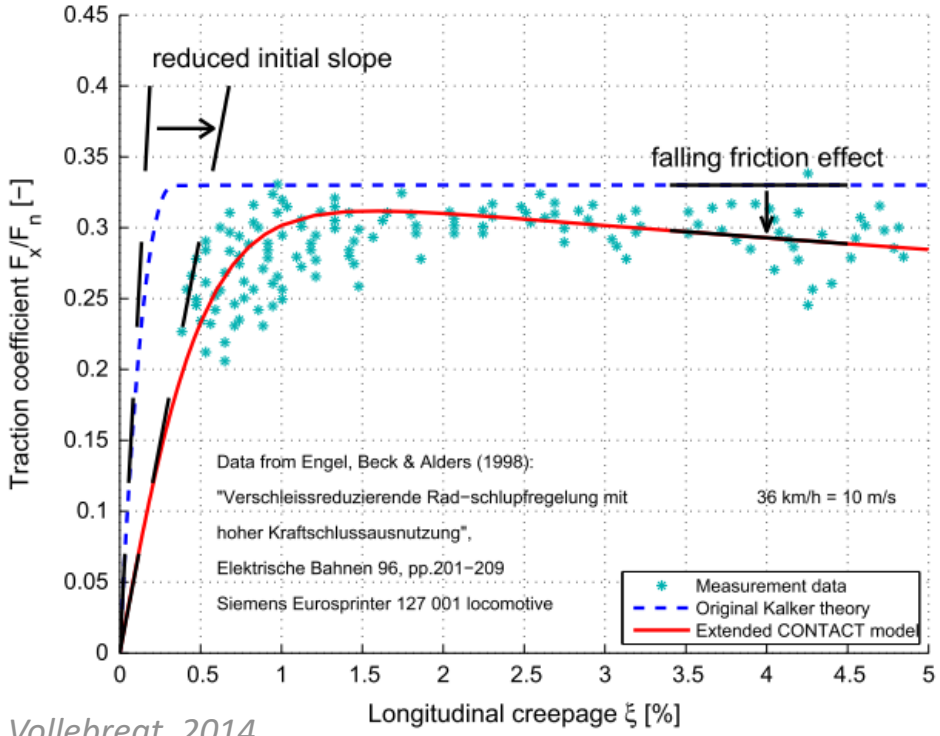

Vollebregt, 2014

Reduced initial slope

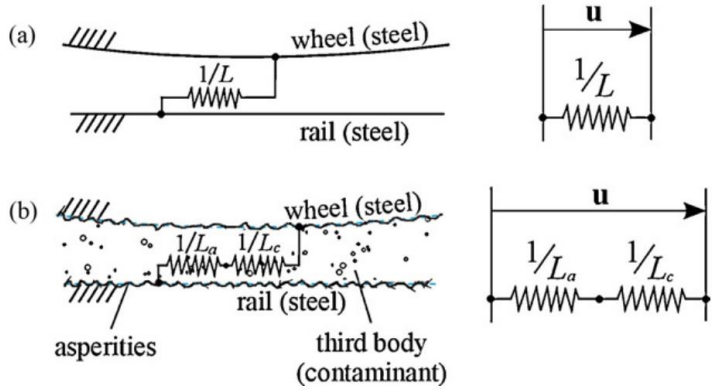

Rovira, 2012

Falling friction effect

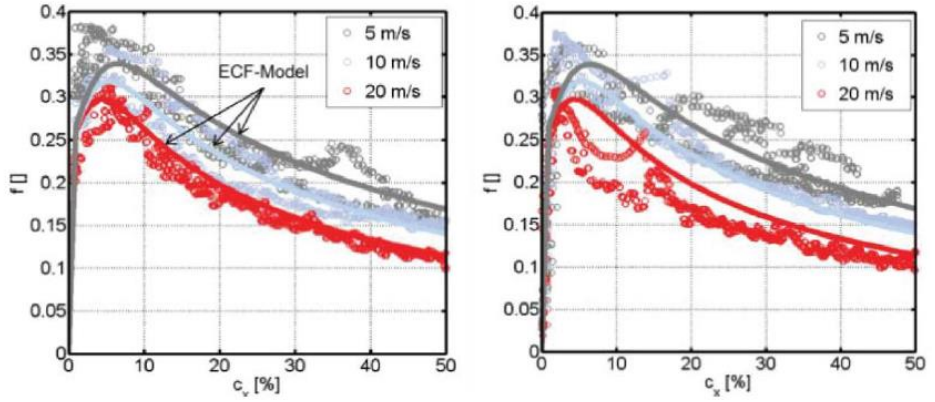

Six, 2015

STATE OF THE ART

Mathematical model | **Elastohydrodynamic effect**

- Combining **EHL** and **asperity contact**

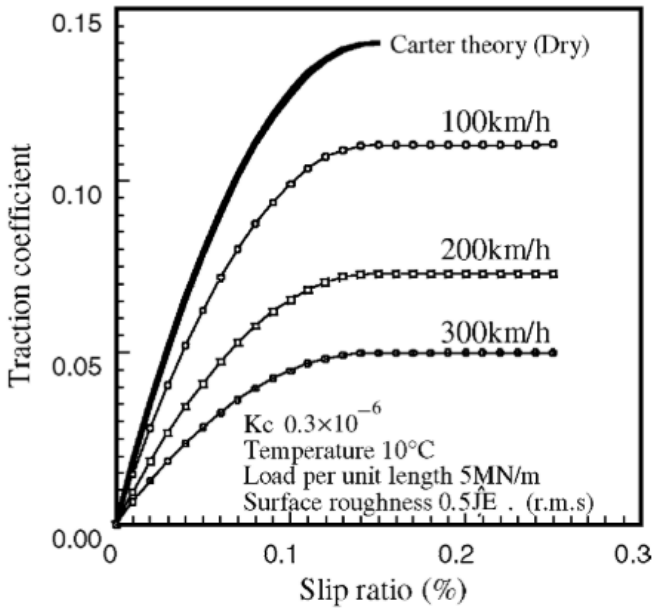

Chen, 2002

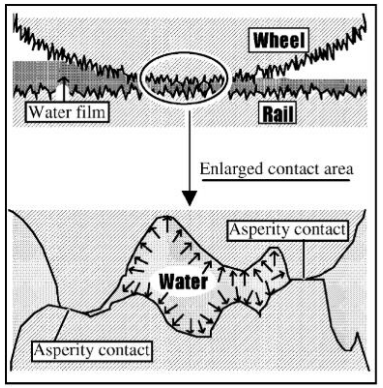

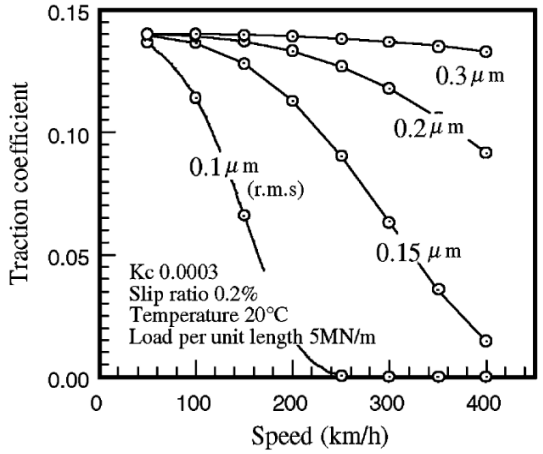

- Statistical asperity models
  - Greenwood and Williamson
  - Zao, Maietta and Chang
  - …

$$\left\{\frac{4}{3}\sqrt{\frac{\bar{\sigma}}{\beta}}\cdot\sqrt{\frac{\pi}{W}}\int_{(\bar{h}/\bar{\sigma})-(G/\xi)}^{(\bar{h}/\bar{\sigma})-(G/\xi)+\omega_1^*}(\varpi)^{3/2}\phi^*(z^*)dz^*+2.\pi.\Omega\sqrt{\frac{\pi}{W}}\int_{(\bar{h}/\bar{\sigma})-(G/\xi)r\omega_1^*}^{\infty}(\varpi)\phi^*(z^*)dz^*\right.$$
$$\left.+.\pi.\Omega\sqrt{\frac{\pi}{W}}\int_{(\bar{h}/\bar{\sigma})-(G/\xi)+\omega_1^*}^{(\bar{h}/\bar{\sigma})-(G/\xi)+r\omega_1^*}\left[1-(1-k)\frac{\ln(r\omega_1^*)-\ln(\varpi)}{\ln r}\right]\times\left[1-2\left(\frac{\varpi-\omega_1^*}{(r-1)\omega_1^*}\right)^3+3\left(\frac{\varpi-\omega_1^*}{(r-1)\omega_1^*}\right)^2\right](\varpi)\phi^*(z^*)dz^*\right\}$$

$$\left\{\frac{4}{3}\sqrt{\frac{\bar{\sigma}}{\beta}}\cdot\sqrt{\frac{\pi}{W}}\int_{(\bar{h}/\bar{\sigma})-(G/\xi)}^{(\bar{h}/\bar{\sigma})-(G/\xi)+\omega_c^*}(\varpi)^{3/2}\phi^*(z)dz+1.03\times\frac{2}{3}\omega_c^{*-0.425}\pi.K.\Omega\sqrt{\frac{\pi}{W}}\int_{(\bar{h}/\bar{\sigma})-(G/\xi)+\omega_c^*}^{(\bar{h}/\bar{\sigma})-(G/\xi)+6\omega_c}(\varpi)^{57/40}\phi^*(z)dz\right.$$
$$\left.+1.4\times\frac{2}{3}\omega_c^{*-0.263}\pi.K.\Omega\sqrt{\frac{\pi}{W}}\int_{(\bar{h}/\bar{\sigma})-(G/\xi)+6\omega_c^*}^{(\bar{h}/\bar{\sigma})-(G/\xi)+110\omega_c^*}(\varpi)^{1263/1000}\phi^*(z)dz+2\pi\Omega\sqrt{\frac{\pi}{W}}\int_{(\bar{h}/\bar{\sigma})-(G/\xi)+110\omega_c^*}^{\infty}(\varpi)\phi^*(z)dz\right\}$$

$$\left\{\frac{4}{3}\cdot\sqrt{\frac{\bar{\sigma}}{\beta}}\sqrt{\frac{\pi}{W}}\int_{(\bar{h}/\bar{\sigma})-(G/\xi)}^{(\bar{h}/\bar{\sigma})-(G/\xi)+1.9\varpi_c}(\varpi)^{3/2}\phi^*(z)dz+\frac{4}{3}\left(\frac{C\pi Y}{2}\right)\sqrt{\frac{\pi}{W}}\int_{(\bar{h}/\bar{\sigma})-(G/\xi)+1.9\varpi_c}^{\infty}\left[\left(\frac{1}{\omega_c}\right)^{1/2}(\varpi)^{3/2}e^{-\frac{1}{4}\left(\frac{\varpi}{\omega_c}\right)^{5/12}}\right.\right.$$
$$\left.\left.+\frac{2.84\times4}{C}\left(1-e^{-0.82\left(\sqrt{\frac{\bar{\sigma}}{\beta}}\sqrt{\varpi}\left(\frac{\varpi}{1.9\omega_c}\right)^{\frac{D}{2}}\right)^{-0.7}}\right)(\varpi)\left(1-e^{-\frac{1}{25}\left(\frac{\varpi}{\omega_c}\right)^{\frac{5}{9}}}\right)\right]\phi^*(z^*)dz^*\right\}$$

Beheshti, 2012

SUMMARY OF LITERATURE REVIEW

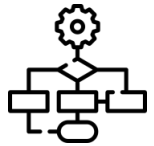

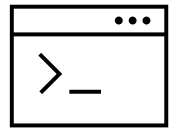

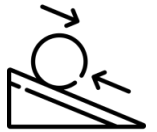

Wheel-rail contact model

Kalker, Six, Meierhofer, Hou, Rovira

Solid-fluid contact model

Chen, Wu, Tomberger

FM/solid FM

Matsumoto, Tomeoka, Ishida, Areiza, Liu, Galas, Hardwick, Lewis, Song

TOR lubricants

Harrison, Lundberg, Liu, Galas , Seo, Hardwick

TOR product shear characteristics

Harrison, Lu, Evans

QUESTIONS

Q1 How to describe a model for top of rail products?

Q3 What are the potential causes of low adhesion for friction modifiers?

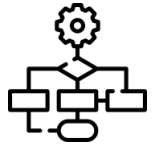

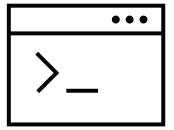

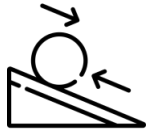

Q2 Does the elastohydrodynamic effect cause low adhesion in top of rail lubricant?

Q4 How do shear properties affect traction curves of top of rail products?

HYPOTHESES

H1

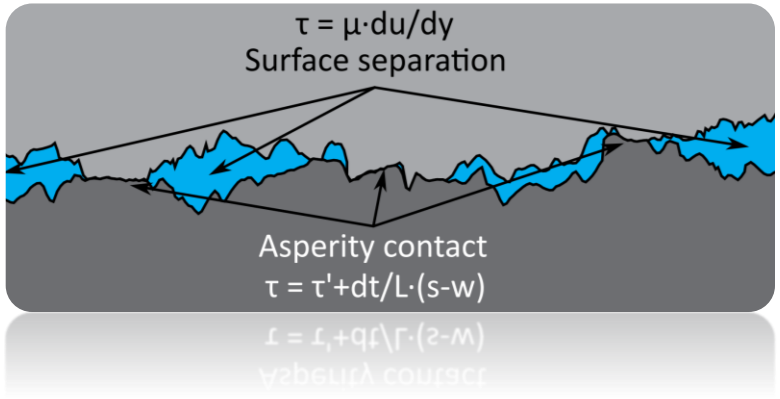

H3.1

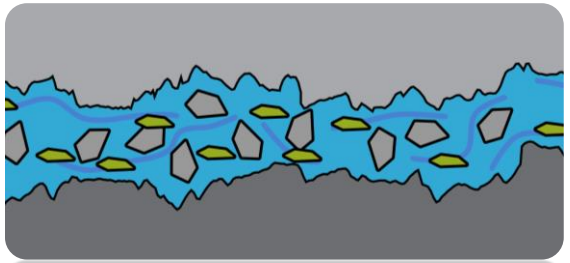

H3.2

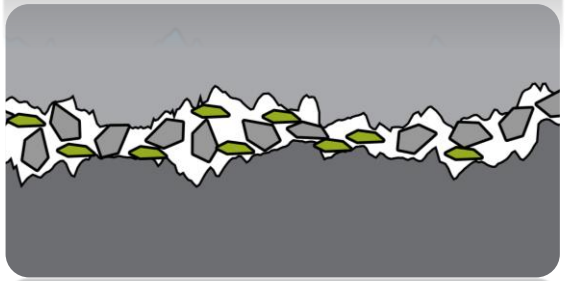

Model

Inputs

Friction

H2.1

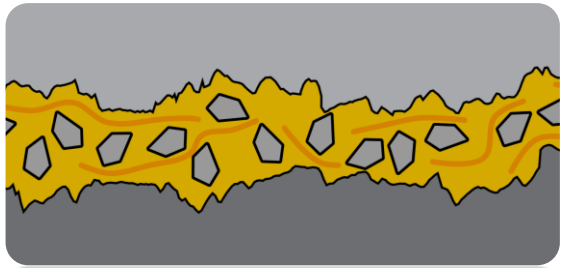

H2.2

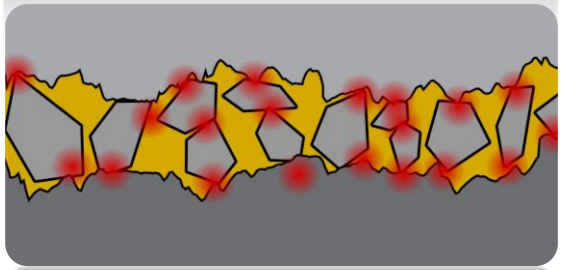

H4

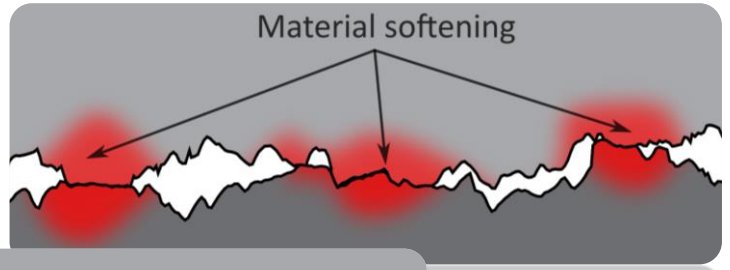

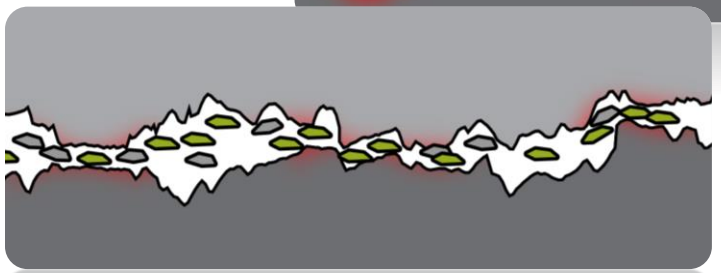

AIM

The aim of this doctoral thesis is to use experimental and modelling methods to clarify the frictional behaviour of top of rail products.

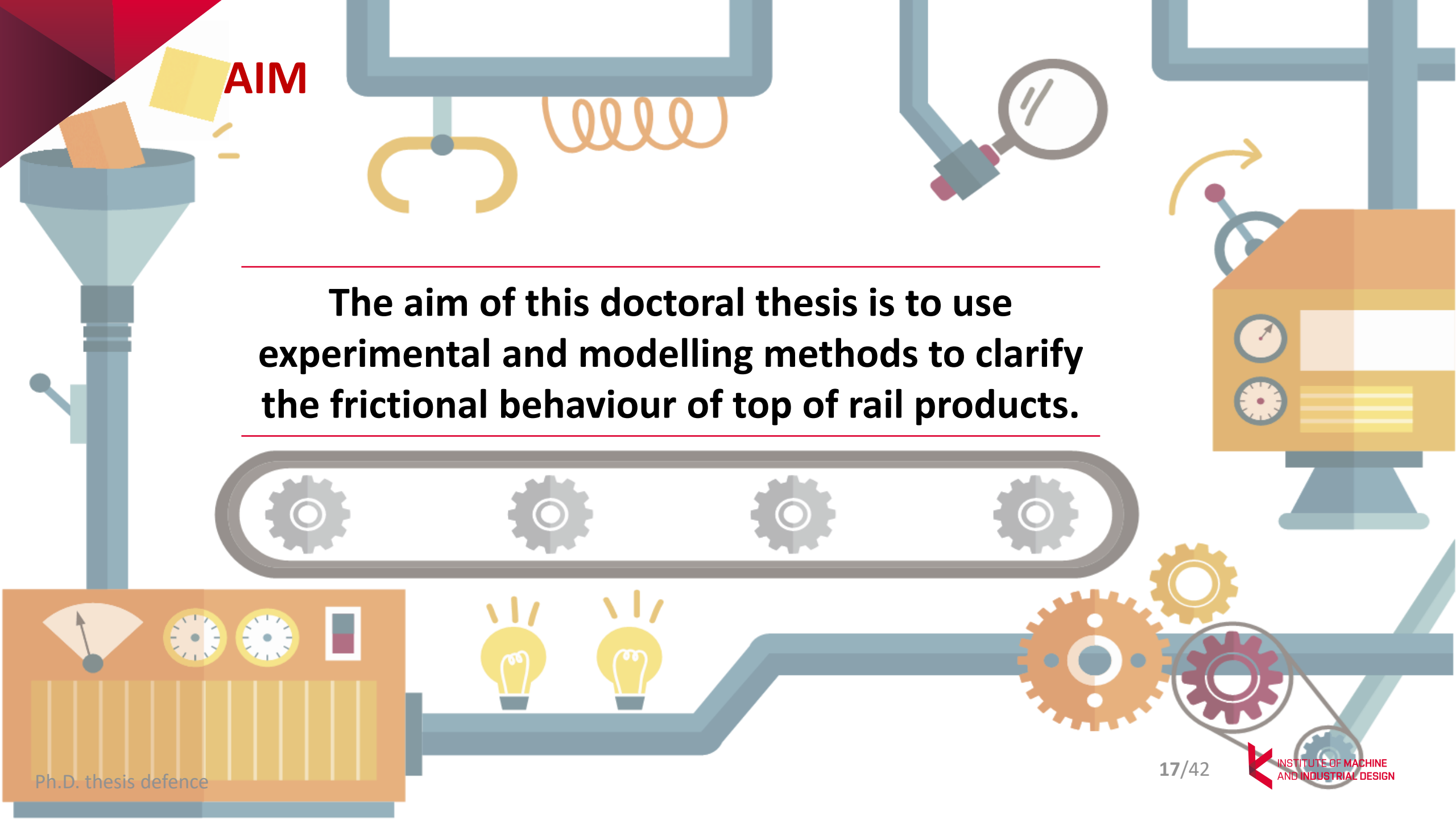

AIM

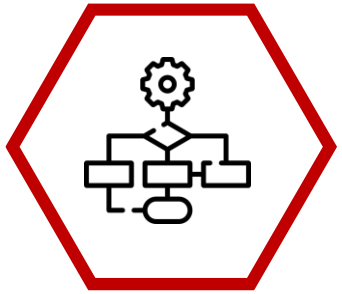

Development of a model for top of rail products, that predicts the coefficient of adhesion across all lubrication regimes.

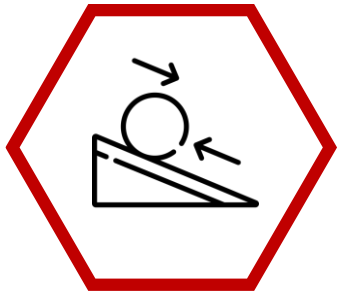

Assessment of low adhesion possibilities for oil-based top of rail lubricants.

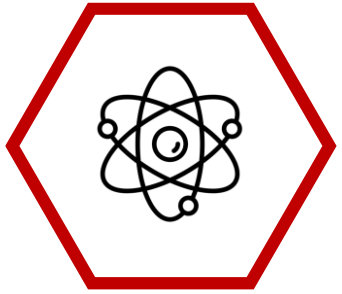

Use of torsion rheometer to assess TOR products and identify inputs for model, and prediction of traction curves for top of rail products.

MATERIALS AND METHODS

Methodology

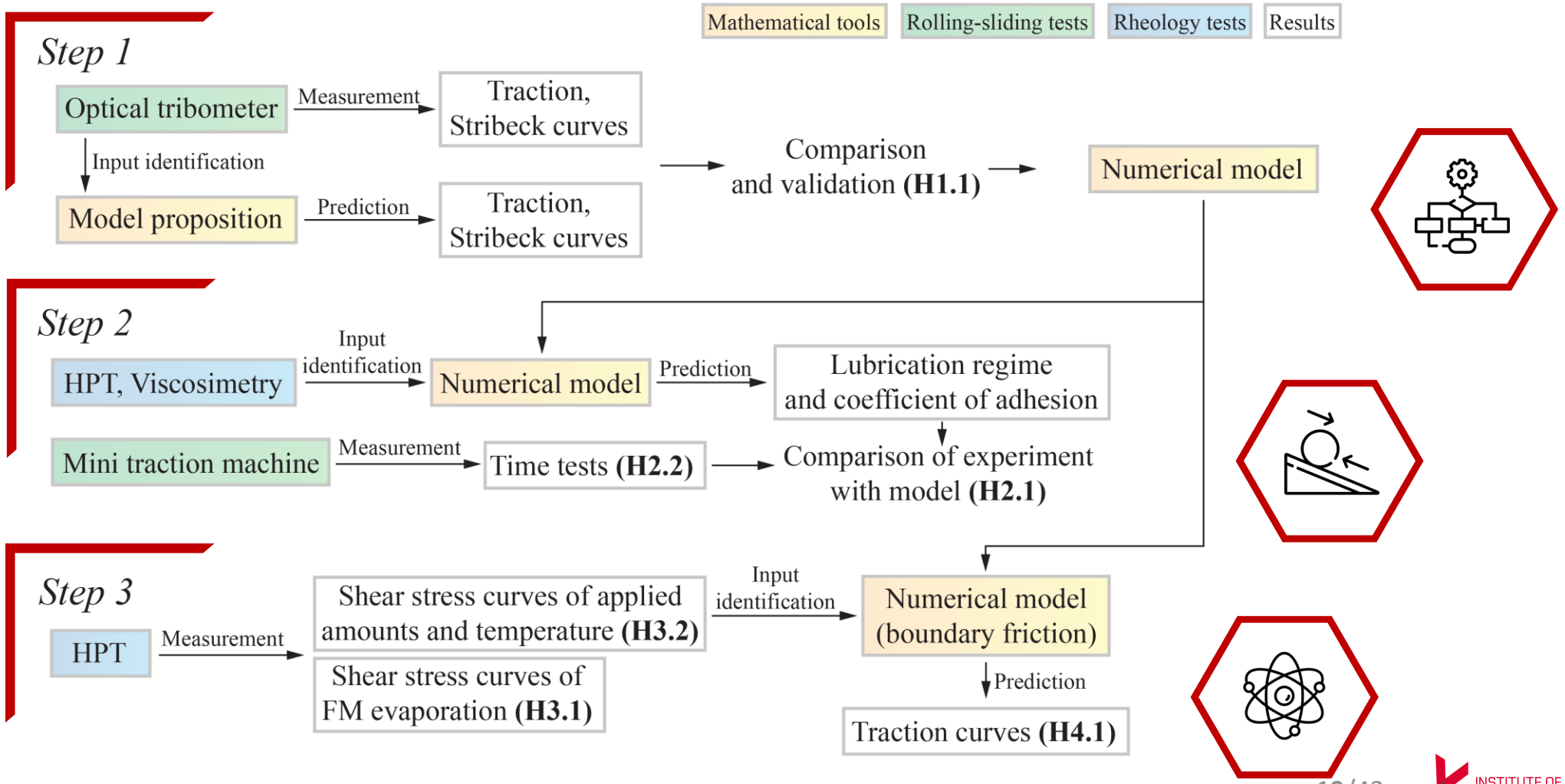

MATERIALS AND METHODS

Mathematical tools		
	Step 1	Comparison and validation **(H1.1)**
	Step 2	Comparison of experiment with model **(H2.1)**
	Step 3	Traction curves **(H4.1)**

Model

- **FASTSIM**-based boundary friction
- **EHL friction** from film thickness formula and viscosity
- Asperity model by **Greenwood and Tripp**

BL friction – extended FASTSIM

$$\tau = \tau' + \frac{\Delta t}{L}[s - w]$$

Six, Meierhofer

$$\tau_{BL} = \tau_{c1} + (\tau_{c2} - \tau_{c1})\left(1 - e^{(-u+\tau_{c1}L_e)/L_p}\right)$$

EHL friction

$$h_c = 5.08U^{0.66}{W_{EHL}}^{-0.21}r_x$$

Chen, Wu

$$h_c = 2.69U^{0.67}G^{0.53}{W_{EHL}}^{-0.067}(1 - 0.61e^{-0.73D})r_x$$

$$\eta = \eta_0 e^{[ln\eta_0+9.67]\left\{\left(1+5.1\cdot10^{-9}p\right)^z-1\right\}}$$

$$\eta = \eta_0 e^{\alpha p}$$

Asperity model

$$p_a = \frac{2}{3}\pi^2 HK^2 F_4\left(\frac{h}{\psi}\right)$$

$$\mu = \frac{\mu_{EHL}W_{EHL} + \mu_{BL}W_{BL}}{W_{EHL} + W_{BL}}$$

Greenwood, Tripp

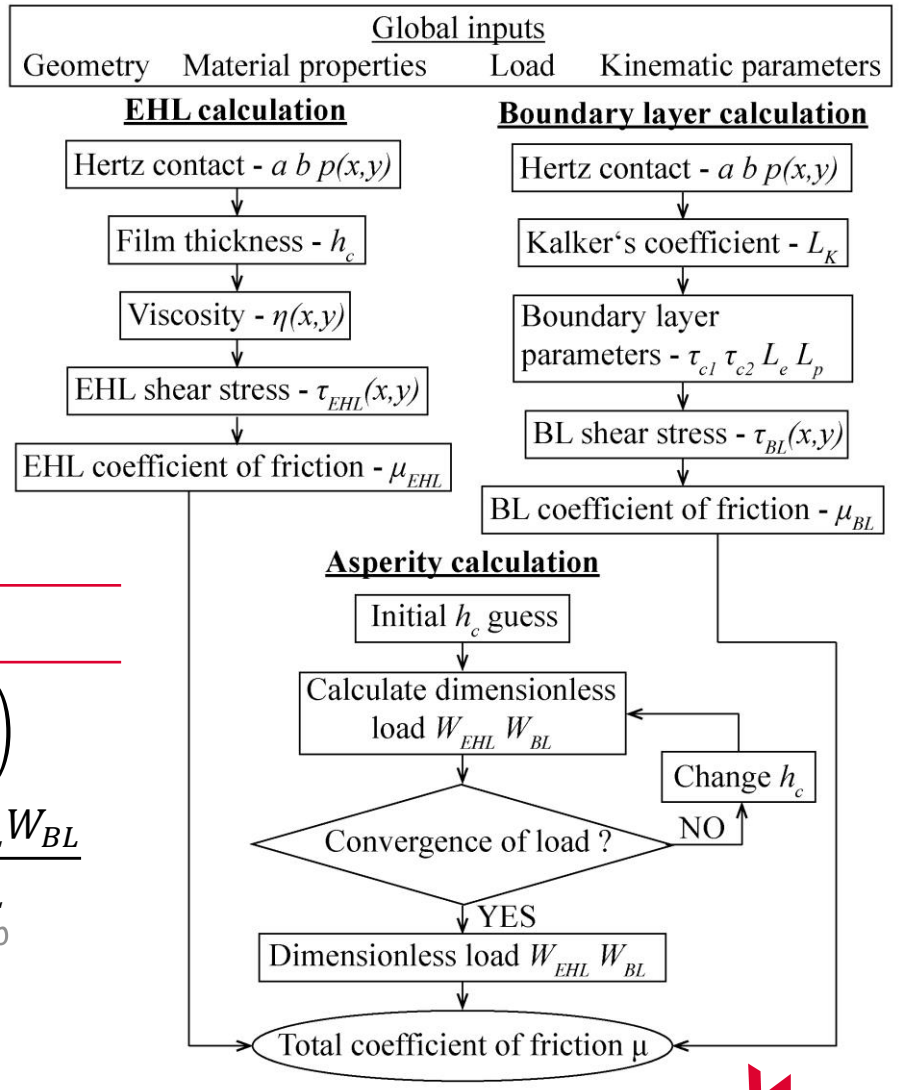

MATERIALS AND METHODS

Rolling-sliding tests | *Step 1* | Comparison and validation **(H1.1)**

Experimental device — Optical tribometer

- Measurement of coefficient of adhesion and lubricant film thickness
- Comparing two types of surface roughness
- Water as a model liquid ($\eta = 10^{-3}$ Pa.s)

Ball diameter	25.4 mm
Material (ball/disc)	AISI 52100/BK7
Maximum Hertzian pressure	0.75 GPa
Slide-to-roll ratio	-10 – 10%
Speed	0 – 2 m/s

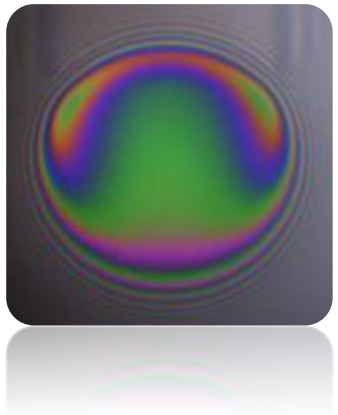

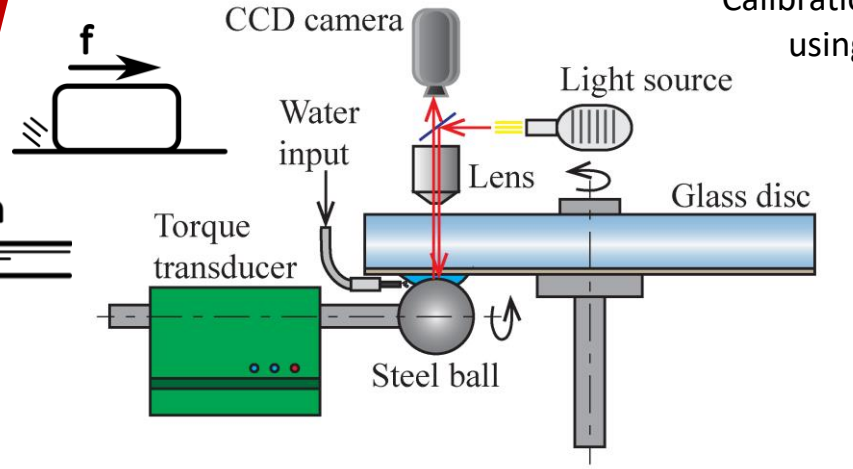

Calibration of model using water

Optical tribometer

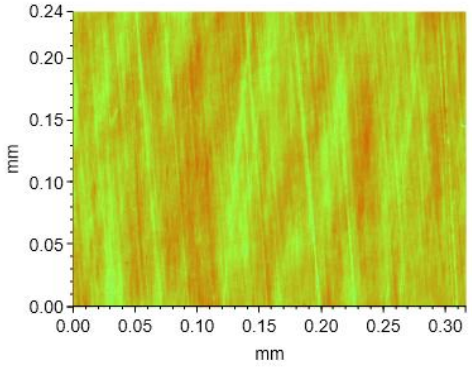

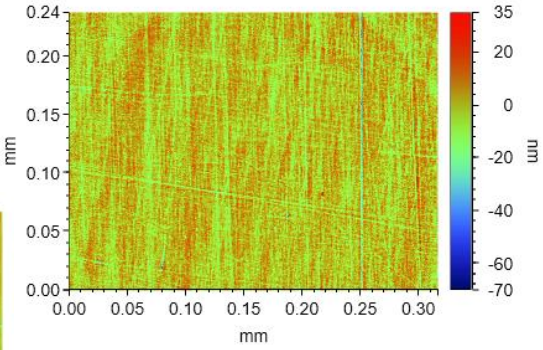

Surface	Roughness standard deviation ψ (nm)	Asperity peak curvature β (mm)	Asperity peak density γ (1/mm²)	*K* (-)
Smooth	8.3	0.301	24 200	0.0605
Rough	9.56	0.373	21 500	0.0767

MATERIALS AND METHODS

Experimental device — Mini traction machine

- Measurement of coefficient of adhesion
- Effect of TORL components
- Time tests under same conditions
- Comparison of **custom TORL** with **commercial** products
- Use of shear properties to determine CoA and regime of lubrication

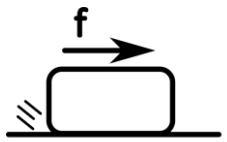

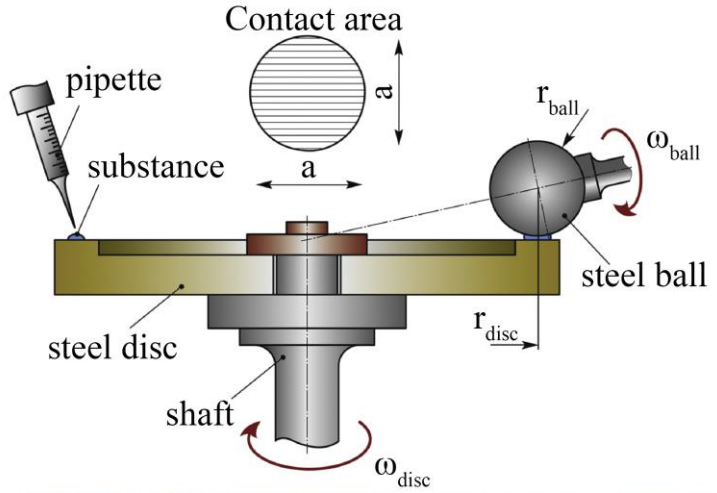

Category	Name	Size (µm)	Mohs (-)
Base medium	Synthetic ester with bentonite thickener		
Friction modifier particles	Aluminium oxide	10, 44 (D99)	9
	Zinc oxide	5 (D99)	4.5
Solid lubricants	Copper sulfide	≈ 5	2.5
	Graphite	7 (D90)	1-2
	Molybdenum disulfide	4.5 (D50)	1-1.5

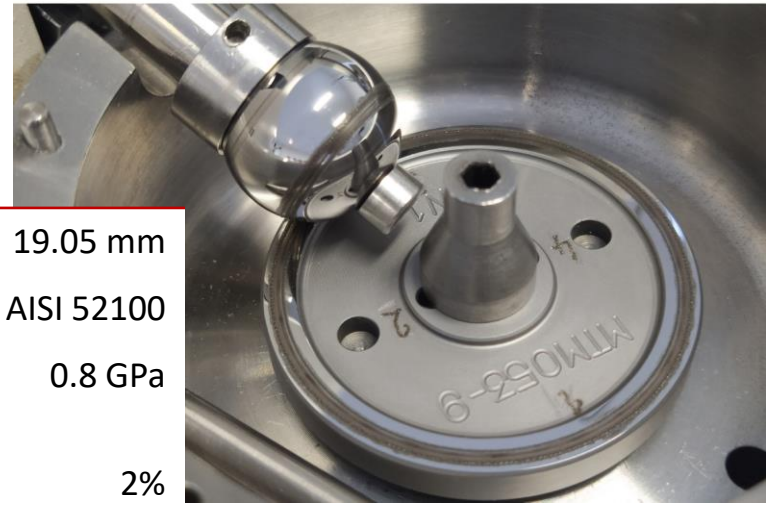

Mini traction machine

Ball diameter	19.05 mm
Specimen material	AISI 52100
Maximum Hertzian pressure	0.8 GPa
Slide-to-roll ratio	2%
Speed	1 m/s
Applied amount of substance	2, 4, 6 µl

MATERIALS AND METHODS

Experimental device | **High pressure torsion**

- Measurement of coefficient of friction/shear stress
- Elastic/pseudo-plastic behavior
- Three types of friction modifiers

Contact area	85 mm^2
Specimen material	DIN 100CrMn6
Contact pressure	0.75 GPa
Displacement rate	1 µm/s
Applied amount of substance	0.1 – 16 µl

Applied TOR-L

Heating module

Rheology tests

Step 2 Comparison of experiment with model **(H2.1)**

Step 3 Shear stress curves of applied amounts and temperature **(H3.2)**

Shear stress curves of FM evaporation **(H3.1)**

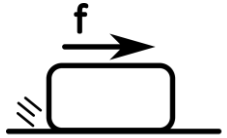

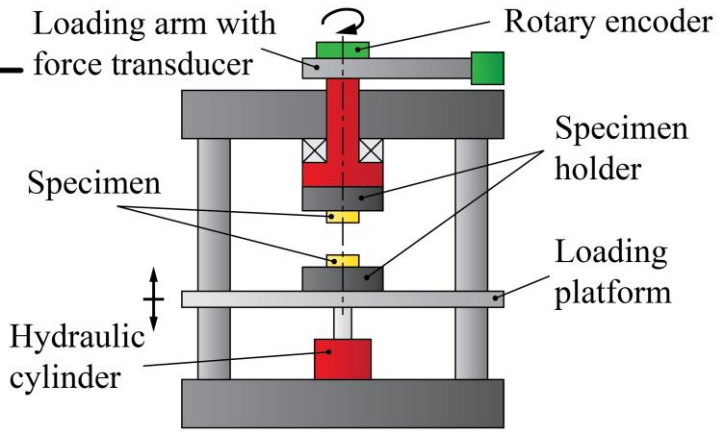

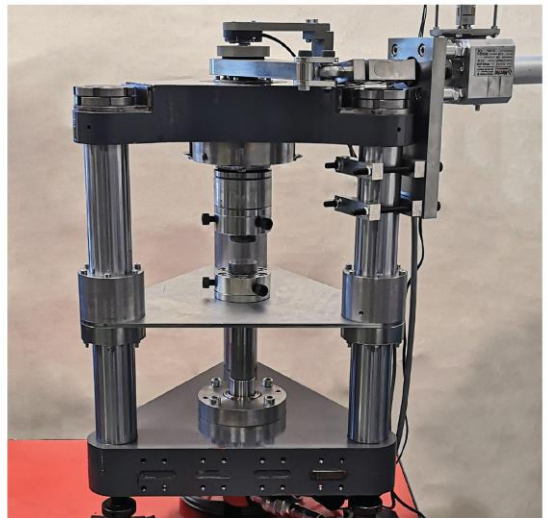

High pressure torsion

RESULTS

Frictional model for top of rail products.

Potential causes of low coefficient of adhesion for friction modifiers.

Effect of elastohydrodynamic regime on adhesion drop after application.

Use of shear properties and model to predict coefficient of adhesion.

RESULTS – Model calibration

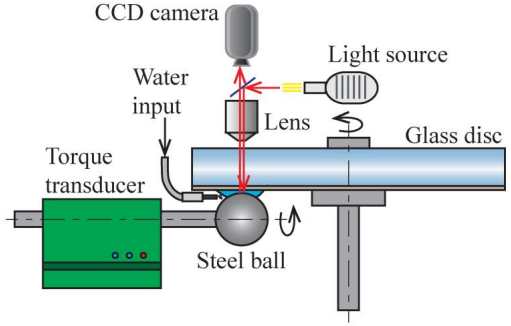

1st phase

Film thickness validation

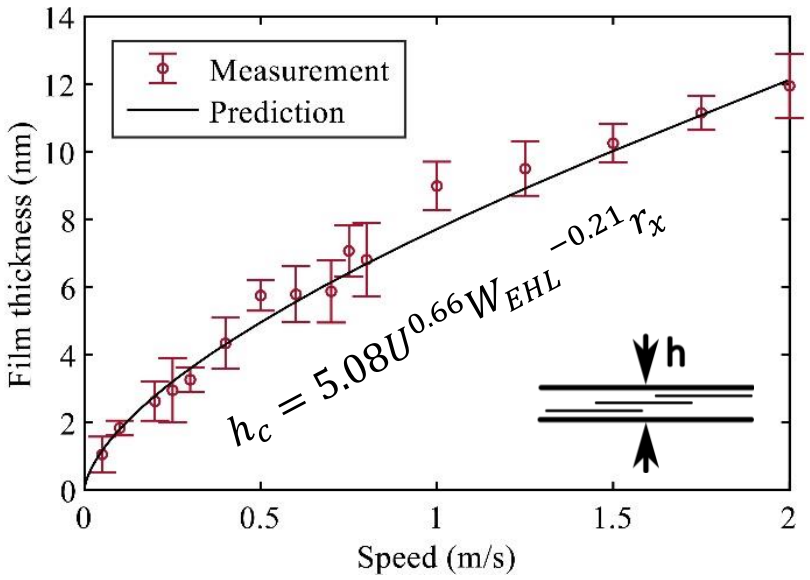

2nd phase

Dry friction calibration

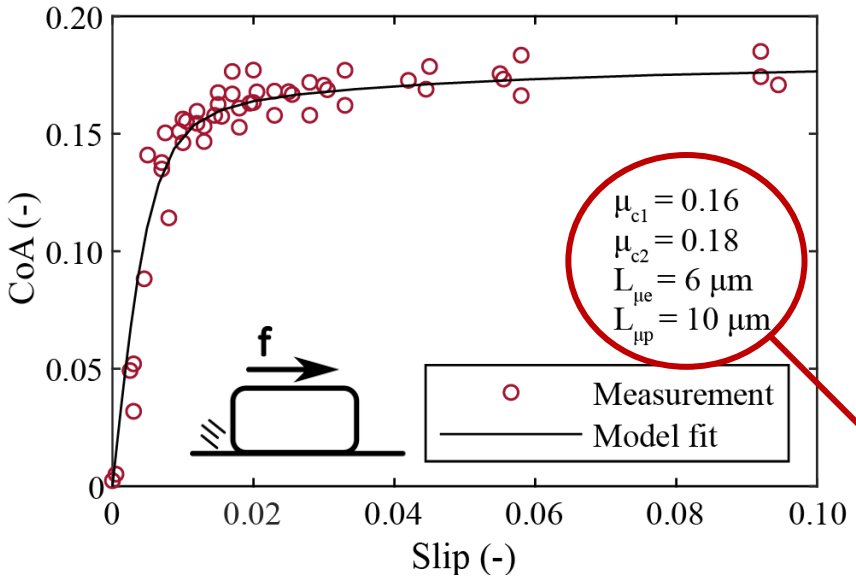

EHL friction equations

$$\eta = 0.001\ Pa \cdot s$$

$$\tau = \eta \cdot w/h_c$$

Boundary friction equations

$$\tau_{c1}(x_i) = (\mu_{c1} p(x_i)) exp(\mu_{c1}{}^T (T(x_i) - T_A))$$

$$\tau_{c2}(x_i) = (\mu_{c2} p(x_i)) exp(\mu_{c2}{}^T (T(x_i) - T_A))$$

$$L_e(x_i) = L_{\mu e}/p(x_i)$$

$$L_p = L_{\mu p}$$

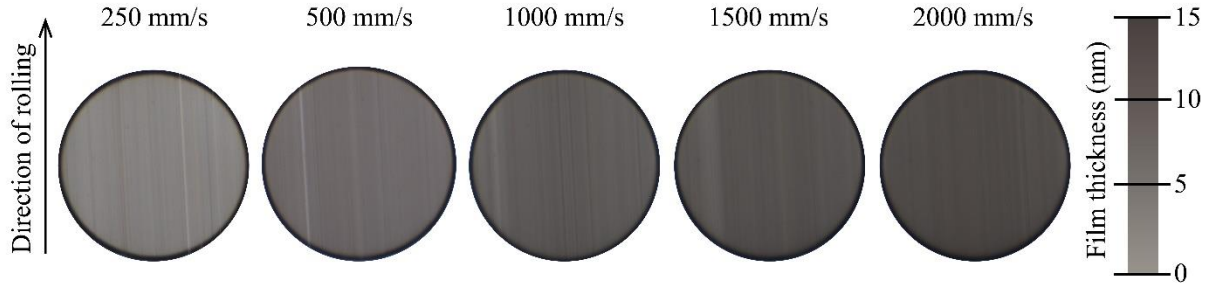

RESULTS – Model validation

Smooth surface

Rough surface

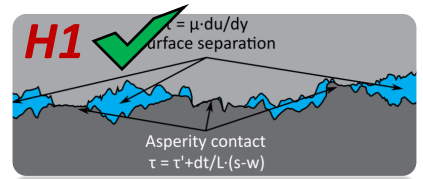

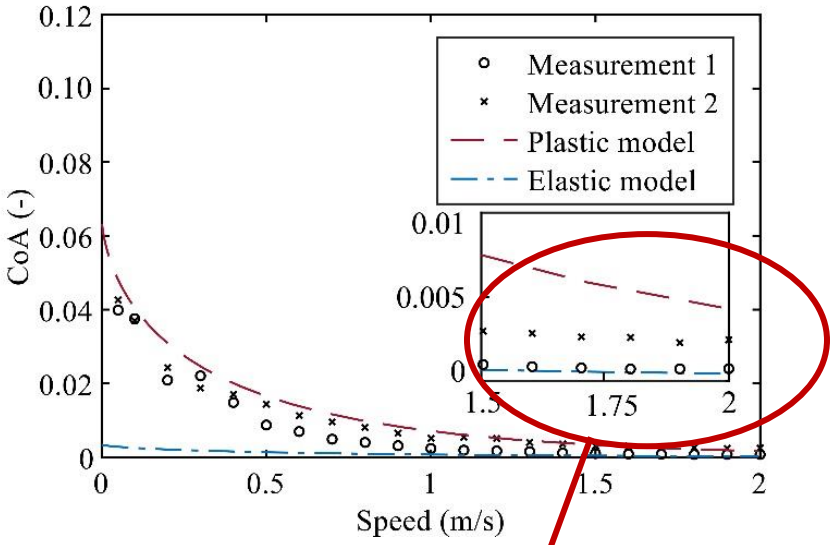

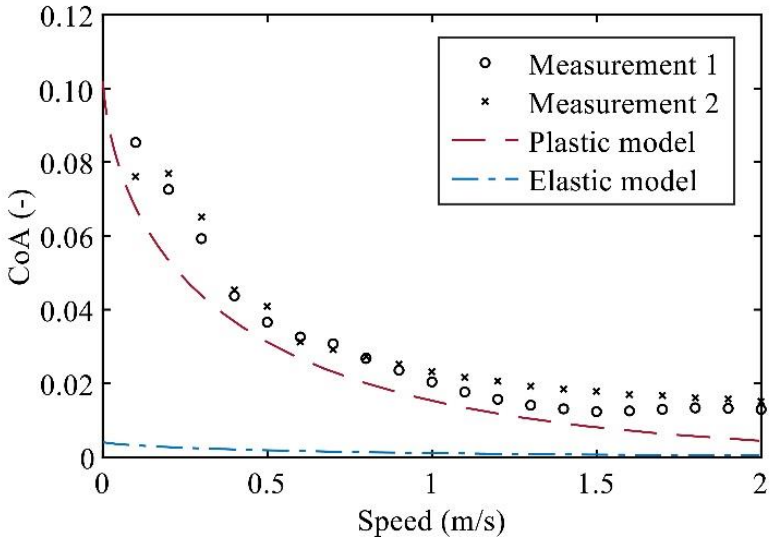

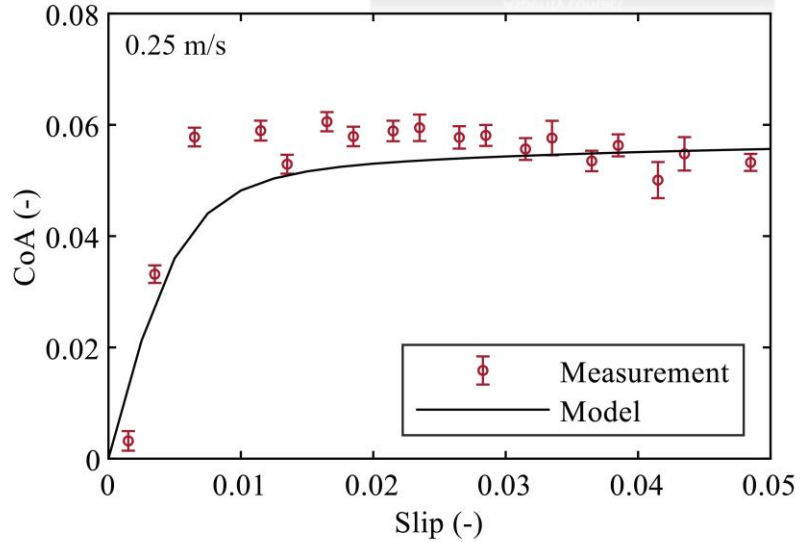

EHL regime

- CoA < 0.003
- *Superlubricity* effects
- Plastic asperity model is more accurate

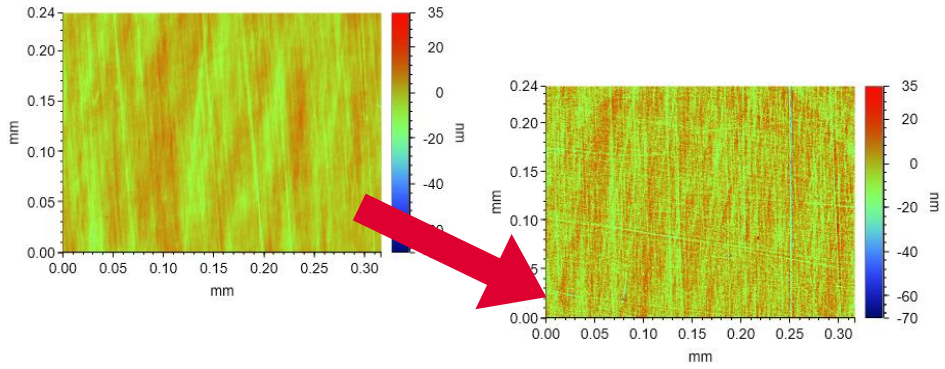

DISCUSSION

- Predicting **wide range of slip and speed conditions** with one calibration
- Relying on correct film thickness prediction → **STARVATION ?**
- Gaussian asperity distribution
- Elastic/Plastic asperity deformation

Q1

Frictional model for top of rail products.

$$\tilde{\Phi}_{CEB}(\bar{h}) \quad \left\{\frac{4}{3}\sqrt{\frac{\bar{\sigma}}{\beta}}\cdot\sqrt{\frac{\pi}{W}}\int_{(\bar{h}/\bar{\sigma})-(G/\xi)+\omega_c^*}^{(\bar{h}/\bar{\sigma})-(G/\xi)+\omega_c^*}(\bar{\omega})^{3/2}\phi^*(z)dz+\pi K\Omega\sqrt{\frac{\pi}{W}}\int_{(\bar{h}/\bar{\sigma})-(G/\xi)+\omega_c^*}^{\infty}(2\bar{\omega}-\omega_c^*)\phi^*(z^*)dz^*\right\}$$

$$\tilde{\Phi}_{ZMC}(\bar{h}) \quad \left\{\frac{4}{3}\sqrt{\frac{\bar{\sigma}}{\beta}}\cdot\sqrt{\frac{\pi}{W}}\int_{(\bar{h}/\bar{\sigma})-(G/\xi)+\omega_1^*}^{(\bar{h}/\bar{\sigma})-(G/\xi)+r\omega_1^*}(\bar{\omega})^{3/2}\phi^*(z^*)dz^*+2.\pi.\Omega\sqrt{\frac{\pi}{W}}\int_{(\bar{h}/\bar{\sigma})-(G/\xi)+r\omega_1^*}^{\infty}(\bar{\omega})\phi^*(z^*)dz^*\right.$$
$$\left.+.\pi.\Omega\sqrt{\frac{\pi}{W}}\int_{(\bar{h}/\bar{\sigma})-(G/\xi)+\omega_1^*}^{(\bar{h}/\bar{\sigma})-(G/\xi)+r\omega_1^*}\left[1-(1-k)\frac{\ln(r\omega_1^*)-\ln(\bar{\omega})}{\ln r}\right]\times\left[1-2\left(\frac{\bar{\omega}-\omega_1^*}{(r-1)\omega_1^*}\right)^3+3\left(\frac{\bar{\omega}-\omega_1^*}{(r-1)\omega_1^*}\right)^2\right](\bar{\omega})\phi^*(z^*)dz^*\right\}$$

$$\tilde{\Phi}_{KE}(\bar{h}) \quad \left\{\frac{4}{3}\sqrt{\frac{\bar{\sigma}}{\beta}}\cdot\sqrt{\frac{\pi}{W}}\int_{(\bar{h}/\bar{\sigma})-(G/\xi)}^{(\bar{h}/\bar{\sigma})-(G/\xi)+\omega_c^*}(\bar{\omega})^{3/2}\phi^*(z)dz+1.03\times\frac{2}{3}\omega_c^{*-0.425}\pi.K.\Omega\sqrt{\frac{\pi}{W}}\int_{(\bar{h}/\bar{\sigma})-(G/\xi)+\omega_c^*}^{(\bar{h}/\bar{\sigma})-(G/\xi)+6\bar{\omega}_c}(\bar{\omega})^{57/40}\phi^*(z)dz\right.$$
$$\left.+1.4\times\frac{2}{3}\omega_c^{*-0.263}\pi.K.\Omega\sqrt{\frac{\pi}{W}}\int_{(\bar{h}/\bar{\sigma})-(G/\xi)+6\omega_c^*}^{(\bar{h}/\bar{\sigma})-(G/\xi)+110\omega_c^*}(\bar{\omega})^{1263/1000}\phi^*(z)dz+2\pi\Omega\sqrt{\frac{\pi}{W}}\int_{(\bar{h}/\bar{\sigma})-(G/\xi)+110\omega_c^*}^{\infty}(\bar{\omega})\phi^*(z)dz\right\}$$

$$\tilde{\Phi}_{JG}(\bar{h}) \quad \left\{\frac{4}{3}\cdot\sqrt{\frac{\bar{\sigma}}{\beta}}\sqrt{\frac{\pi}{W}}\int_{(\bar{h}/\bar{\sigma})-(G/\xi)}^{(\bar{h}/\bar{\sigma})-(G/\xi)+1.9\bar{\omega}_c}(\bar{\omega})^{3/2}\phi^*(z)dz+\frac{4}{3}\left(\frac{C\pi\gamma}{2}\right)\sqrt{\frac{\pi}{W}}\int_{(\bar{h}/\bar{\sigma})-(G/\xi)+1.9\bar{\omega}_c}^{\infty}\left[\left(\frac{1}{\bar{\omega}_c}\right)^{1/2}(\bar{\omega})^{3/2}e^{-\frac{1}{4}\left(\frac{\bar{\omega}}{\bar{\omega}_c}\right)^{5/12}}\right.\right.$$
$$\left.\left.+\frac{2.84\times4}{C}\left(1-e^{-0.82\left(\sqrt{\frac{\bar{\sigma}}{\beta}}\sqrt{\bar{\omega}}\left(\frac{\bar{\omega}}{1.9\bar{\omega}_c}\right)^{\frac{D}{2}}\right)^{-0.7}}\right)(\bar{\omega})\left(1-e^{-\frac{1}{25}\left(\frac{\bar{\omega}}{\bar{\omega}_c}\right)^{\frac{3}{2}}}\right)\right]\phi^*(z^*)dz^*\right\}$$

Smooth surface (pre-measurement)

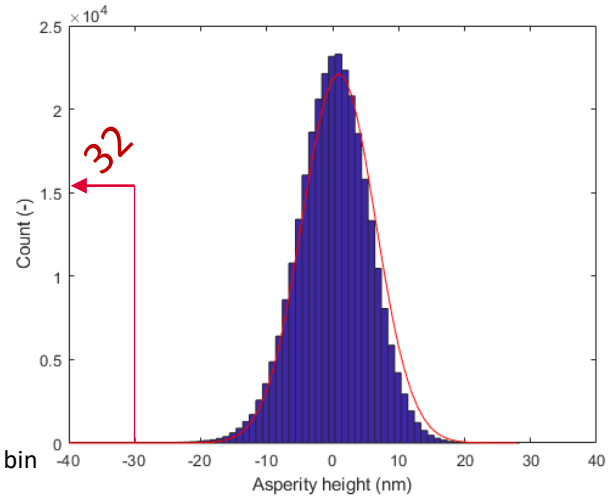

Rough surface (pre-measurement)

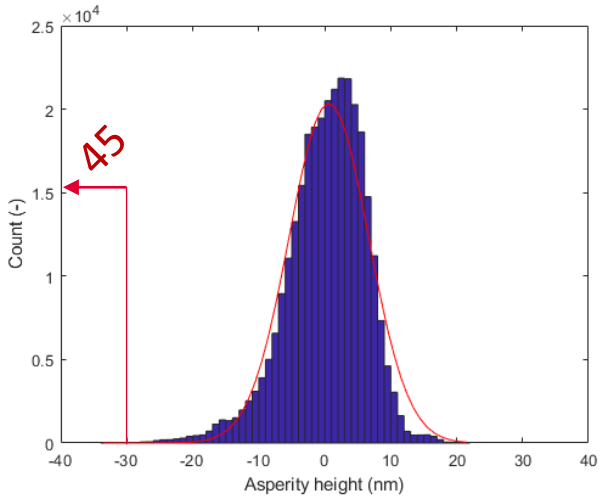

Lightly worn surface (post-measurement)

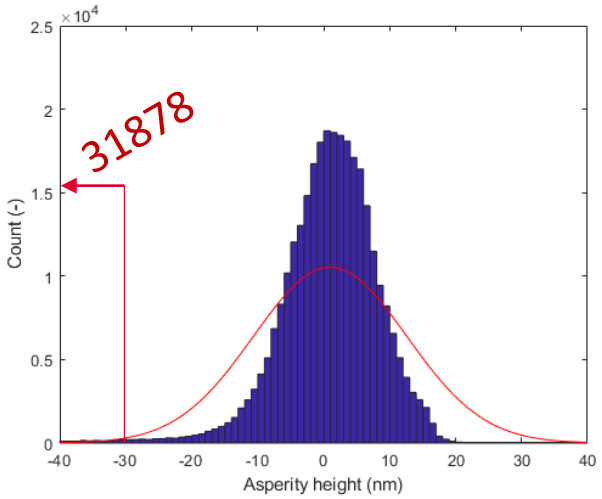

1 nm bin

RESULTS

Frictional model for top of rail products.

Potential causes of low coefficient of adhesion for friction modifiers.

Effect of elastohydrodynamic regime on adhesion drop after application.

Use of shear properties and model to predict coefficient of adhesion.

RESULTS – TORL lubrication regime

Custom TORL and use in modelling

- Commercial TORL **overlubricate** the contact earlier than prepared substances
- The amount of solid lubricant mainly controlled the **substance viscosity**

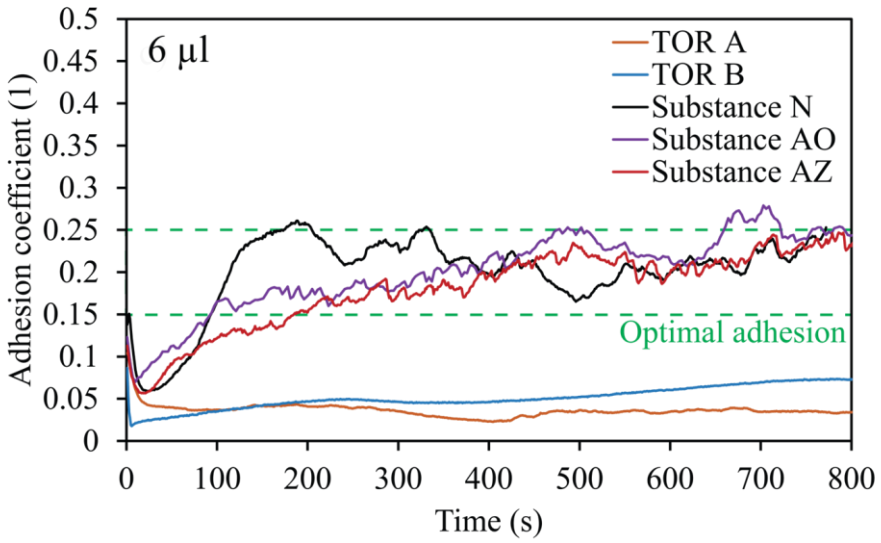

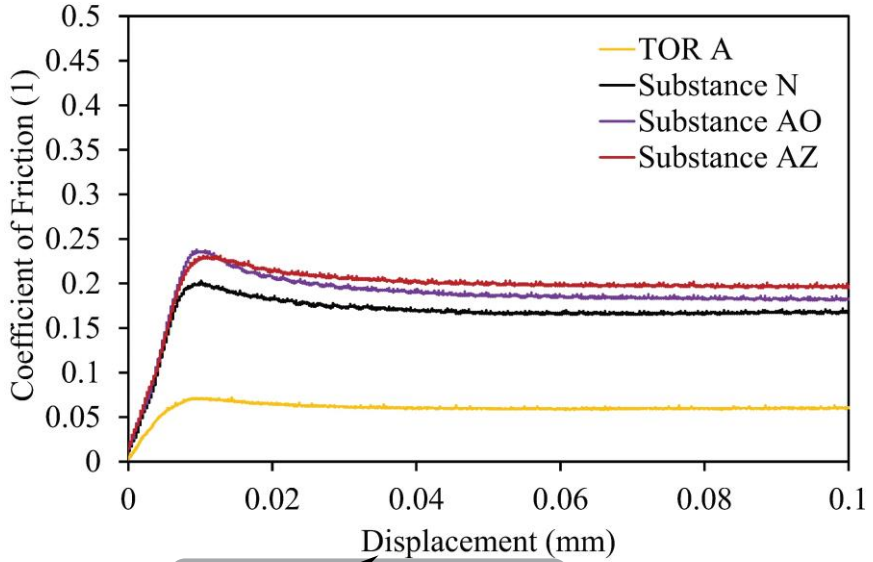

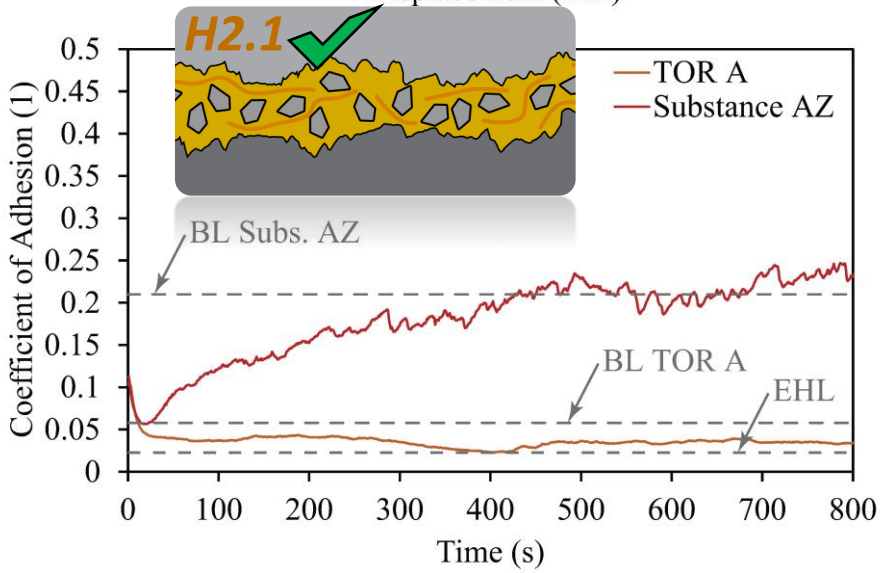

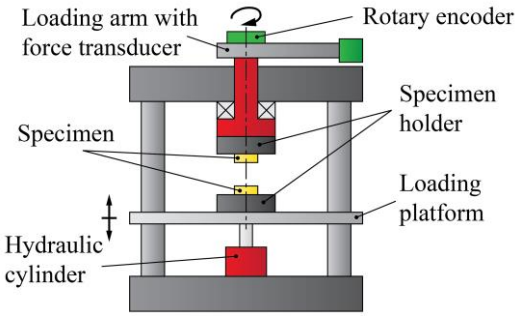

Transition from displacement to slip

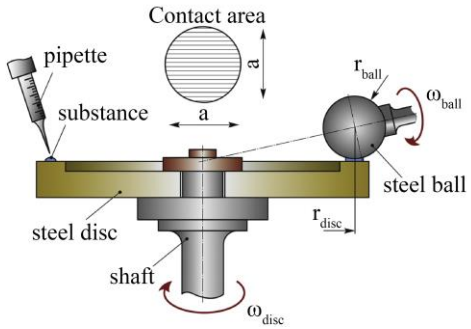

RESULTS – TOL particle influence

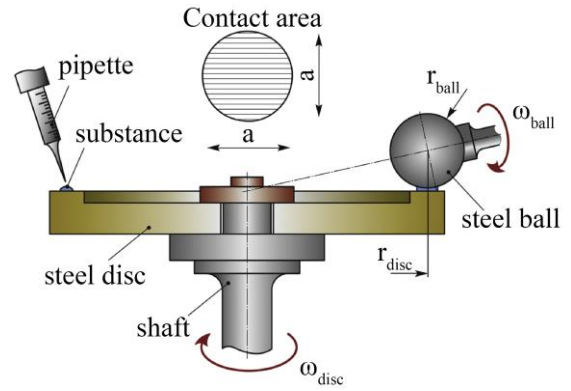

Evaluating the effect of solid particles in TORL

- Initially, hard particles do not provide enough solid-solid interaction
- Zinc oxide and copper sulphide are **ineffective** in base medium
- Base oil **increases** the lubrication properties of MoS_2 and graphite

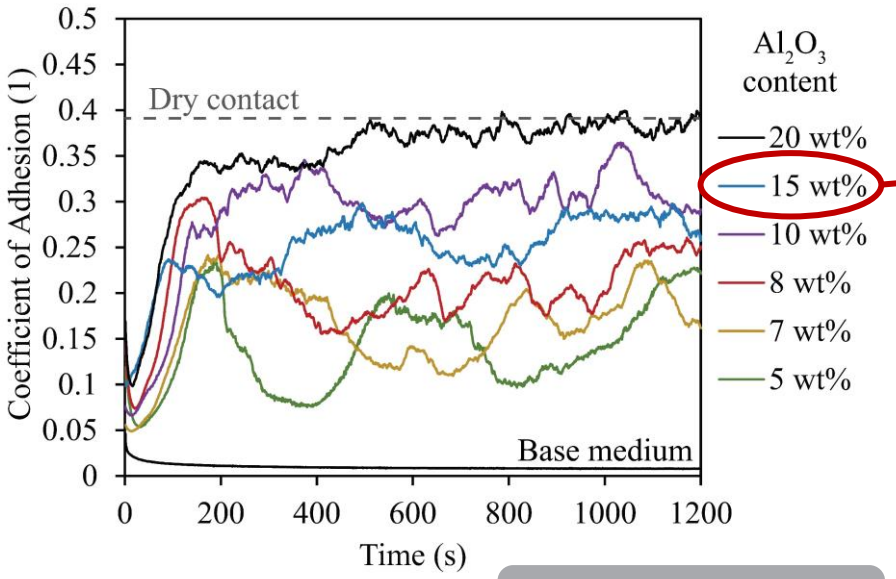

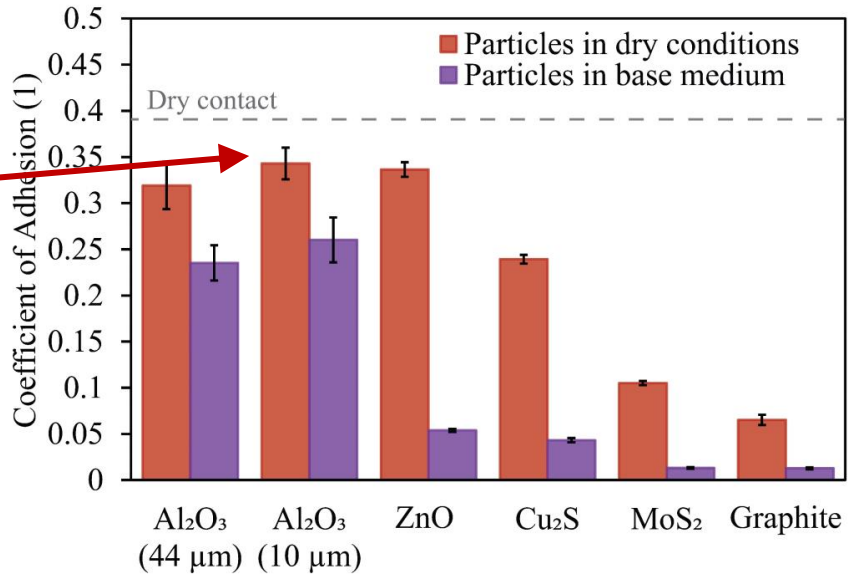

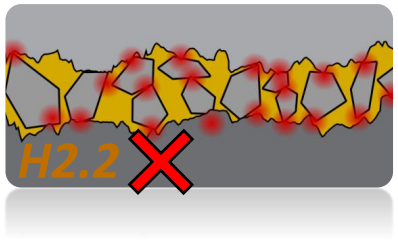

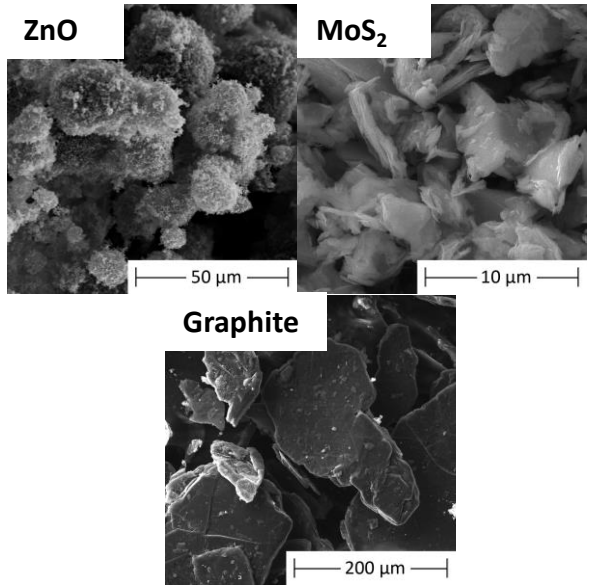

DISCUSSION

Q2

Effect of elastohydrodynamic regime on adhesion drop after application.

Effect of TORL composition

- Medium-hardness particles are **not effective** in TOR lubricant
- Particle content or size **does not eliminate initial drop**
- Bearing steel might suppress particles from embedding

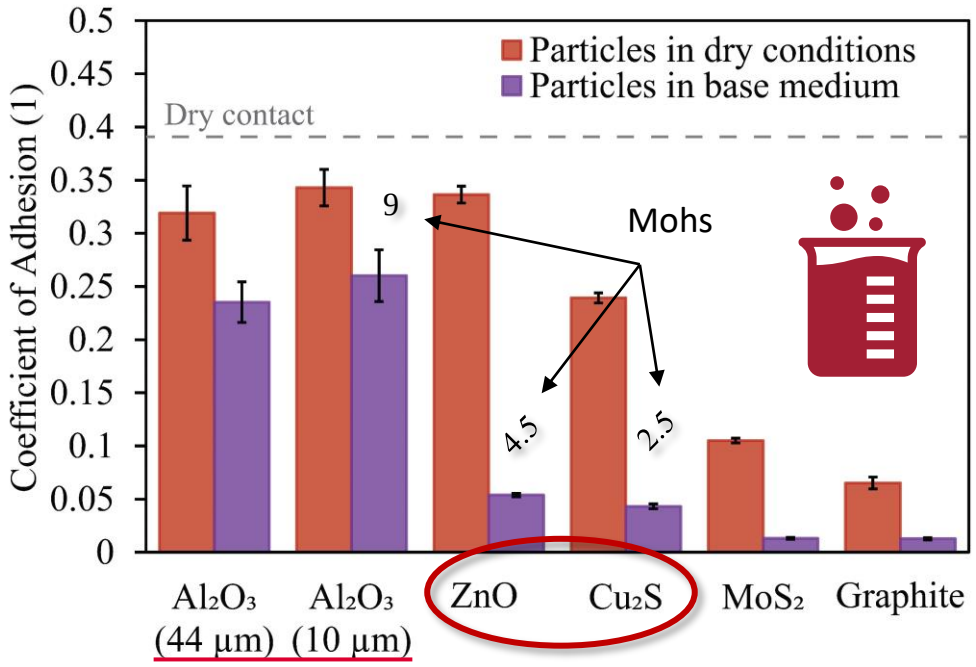

Conditions where particles are ineffective

- Possible scaling issues (particle size to contact area)
- Different surface roughness and material properties

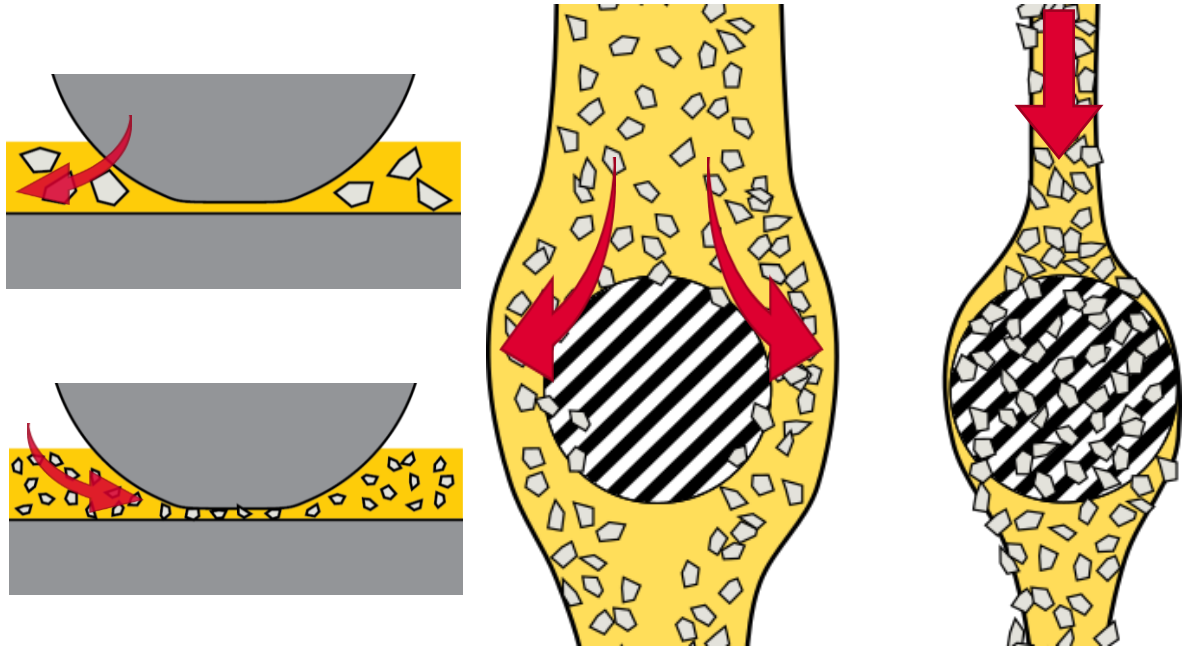

RESULTS

Frictional model for top of rail products.

Potential causes of low coefficient of adhesion for friction modifiers.

Effect of elastohydrodynamic regime on adhesion drop after application.

Use of shear properties and model to predict coefficient of adhesion.

RESULTS – TOR products

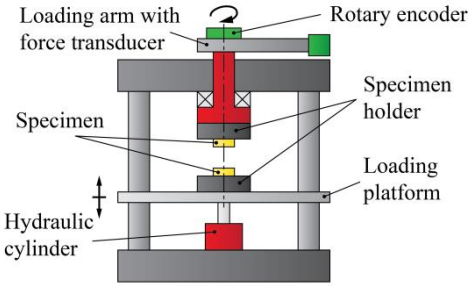

Evaluating shear response of TOR products

- More than 2 µl(mg) applied **does not** lower CoF further
- The relationship between applied amount and CoF follows **similar trend** for all products
- The application strategy and field use needs to be considered

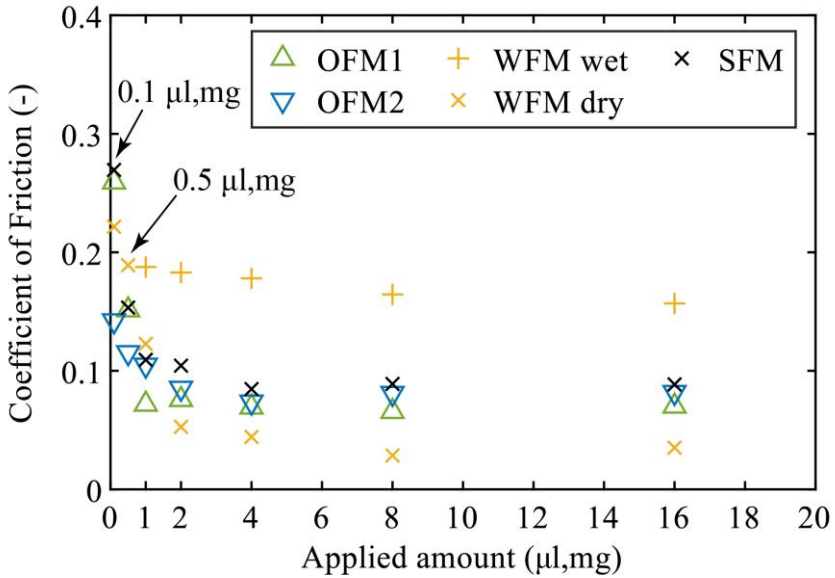

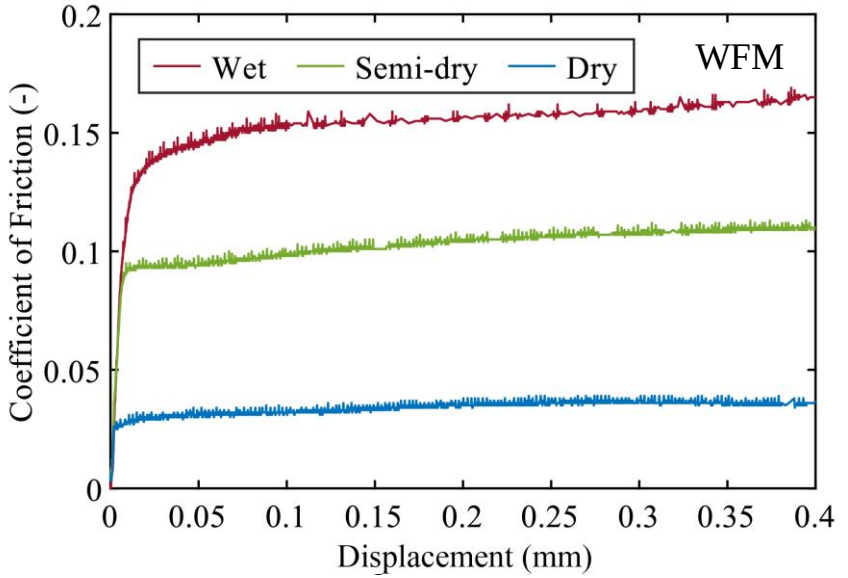

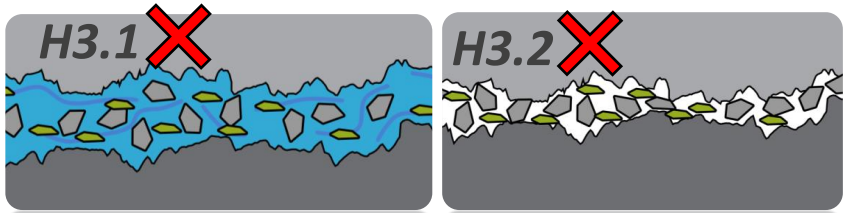

DISCUSSION

Q3

Potential causes of low coefficient of adhesion for friction modifiers.

- **Friction modifier**
  - In dry state, particles cannot get squeezed out
  - In wet state, squeezing out removes any excessive amount
- **Solid FM** is frictionally the same, but overapplication in the field is **not easy**

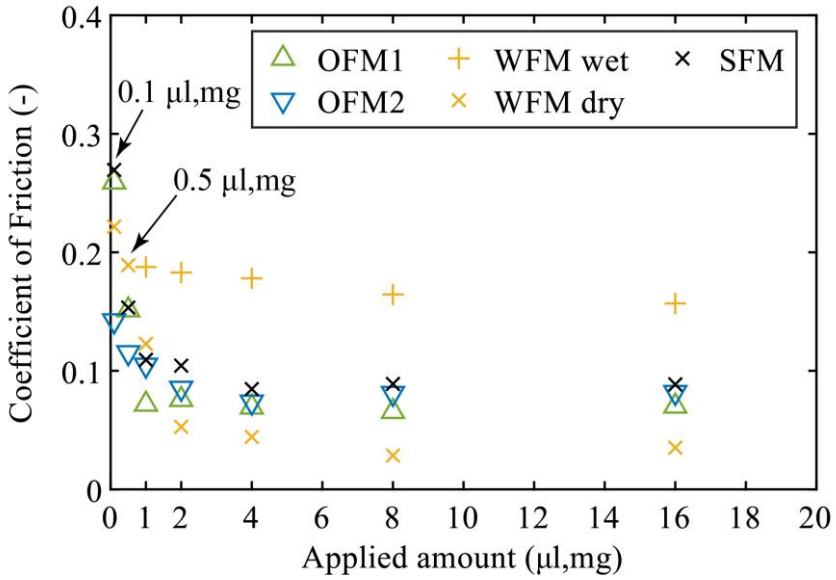

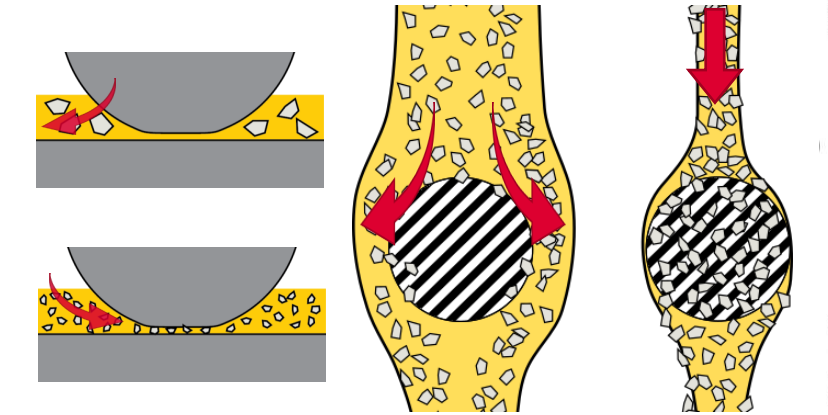

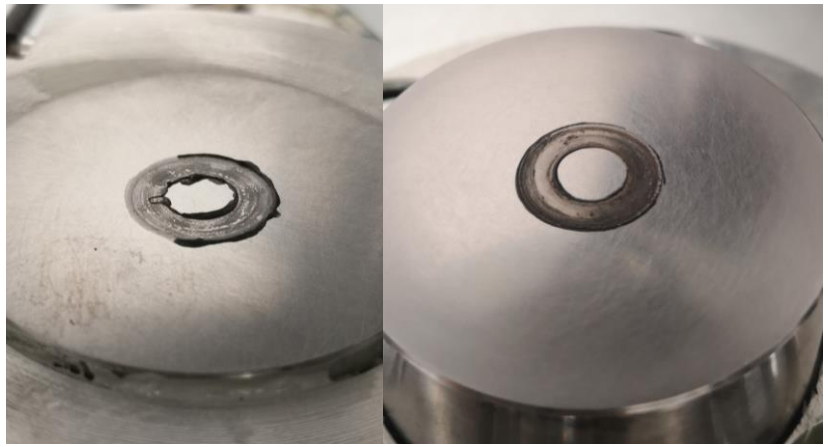

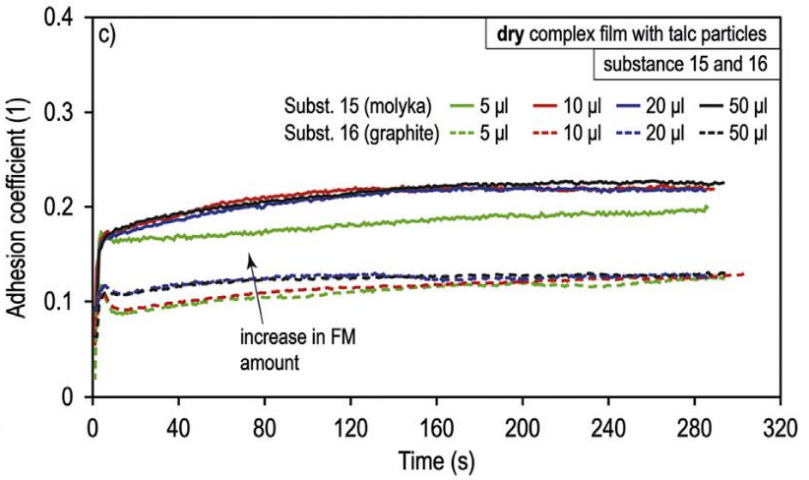

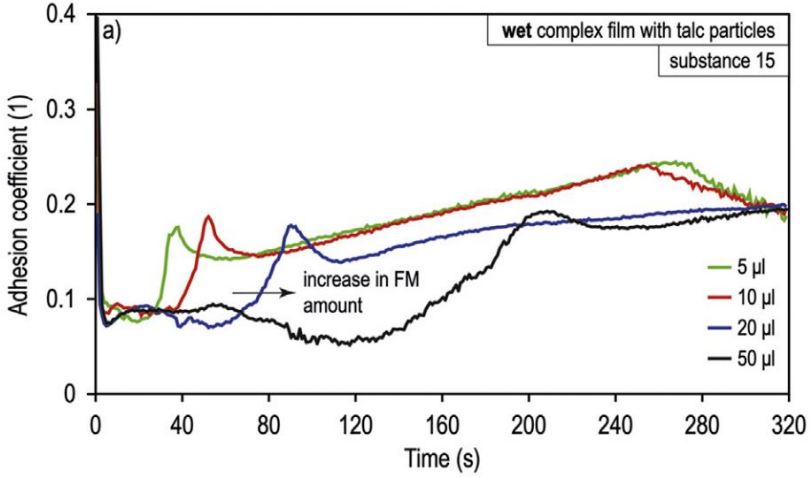

Galas, 2018

RESULTS

Frictional model for top of rail products.

Potential causes of low coefficient of adhesion for friction modifiers.

Effect of elastohydrodynamic regime on adhesion drop after application.

Use of shear properties and model to predict coefficient of adhesion.

RESULTS – TOR products rheology

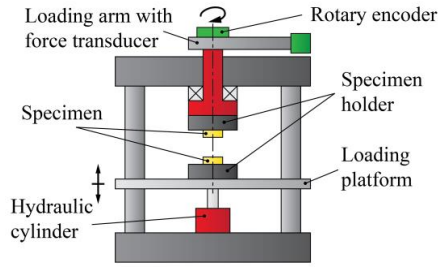

Identification of TOR material parameters

- Elastic and pseudo-plastic behavior
- Temperature influence

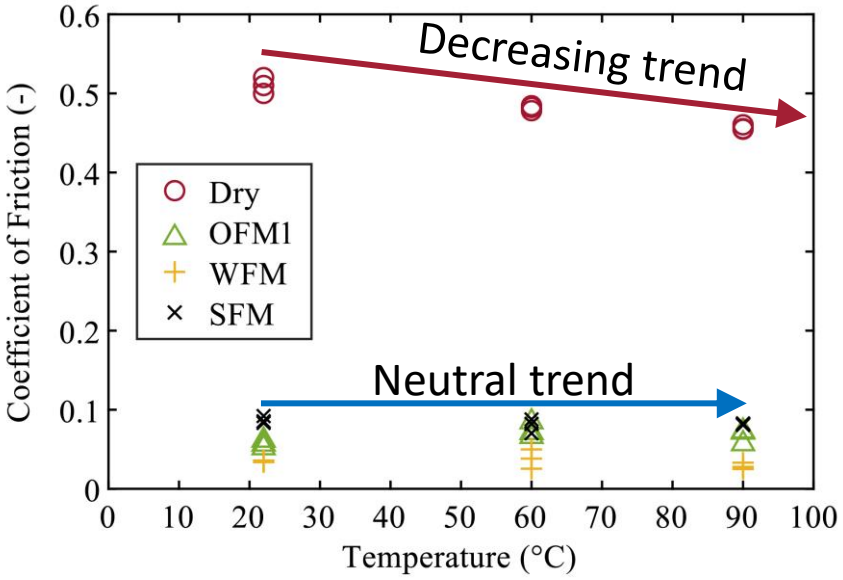

	Dry	OFM1 0.5 µl	WFM dry 0.5 µl	SFM 0.1 mg
k_1,k_2 (1/°C)	-0.0016	0.0005	-0.001	-0.0005

- Increase in temperature affected **only dry conditions**
- No positive trend was observed

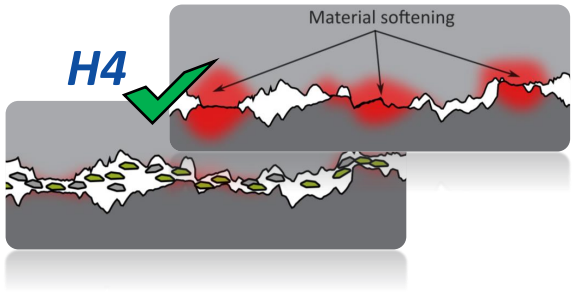

Simulation of traction curves

- p_{max} = 790 MPa
- v = 10 m/s
- S = 38 mm^2

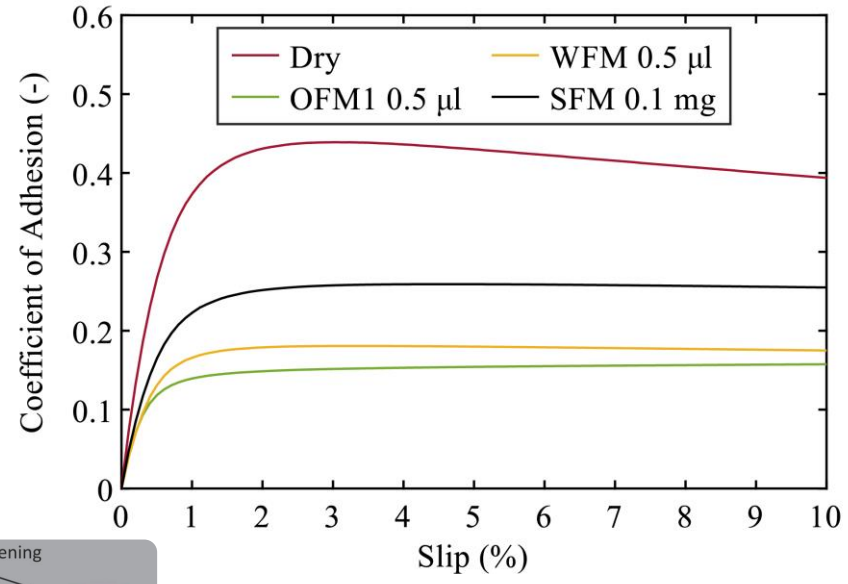

DISCUSSION

Q4

Use of shear properties and model to predict coefficient of adhesion, overcoming transient effects.

- Rheological tests of TOR did not show positive/negative trends (Evans, Harrison)
- Increased temperature without TOR – **negative trend**
- Increased temperature with TOR – **neutral trend**
- **Positive trend** as a result of TOR layer removal ?

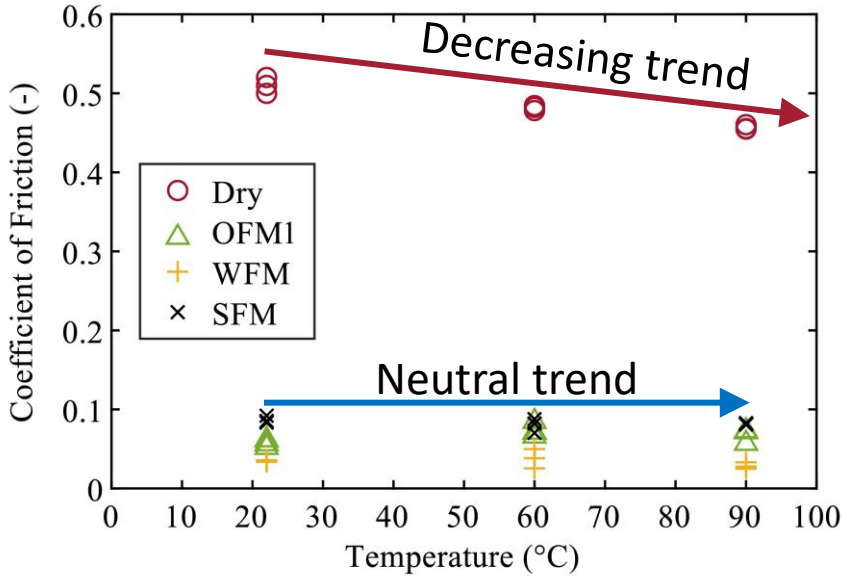

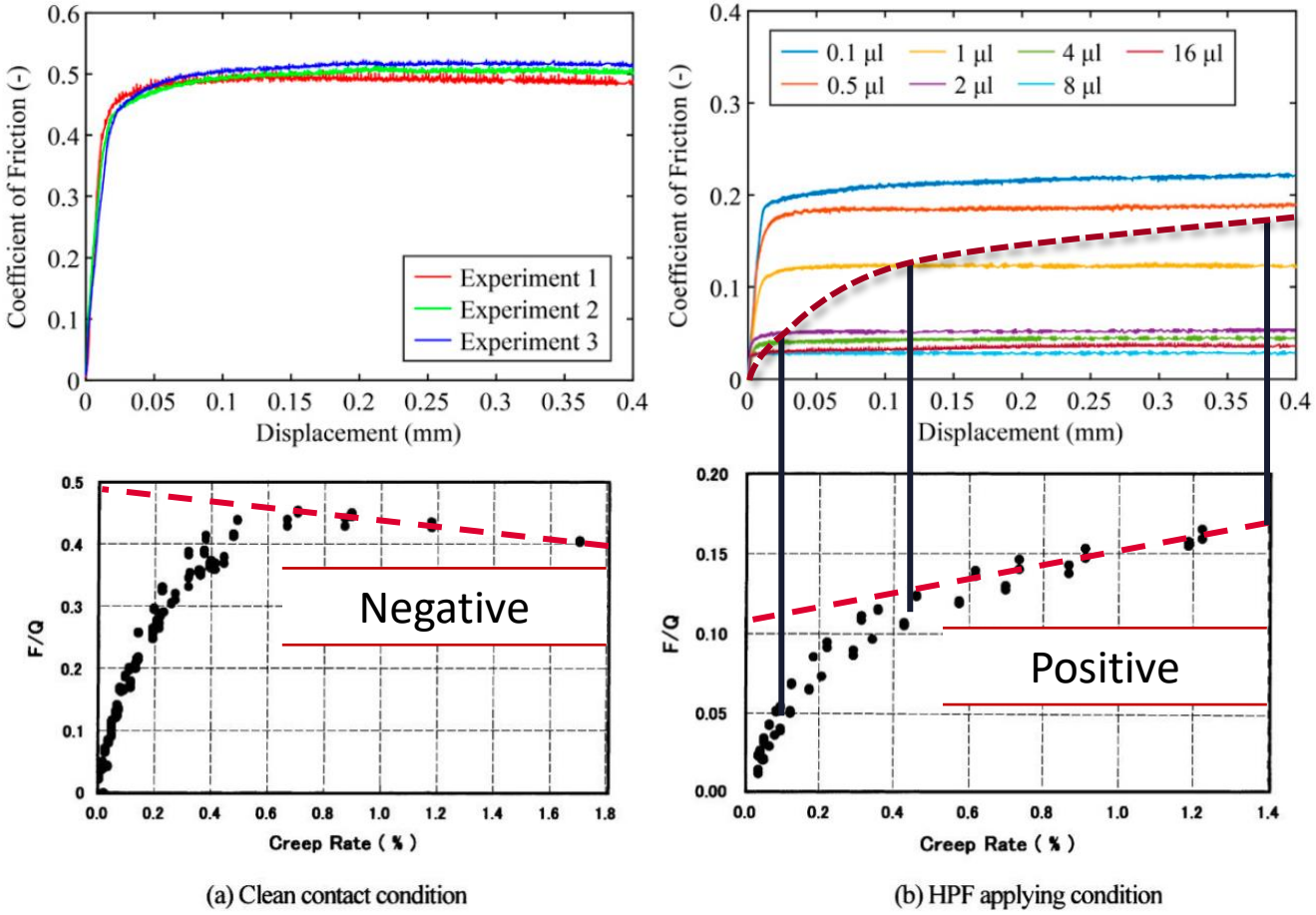

(a) Clean contact condition

(b) HPF applying condition

CONCLUSION

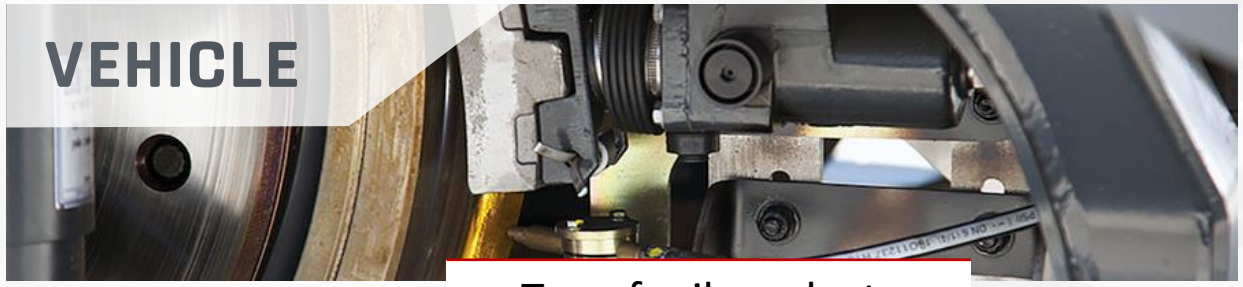

Top of rail products

Top of rail lubricant

- Hardness and size of particles is very important
- Difficult to suppress initial drop after application
- Possible scaling issues with experimental device

Friction modifier

- Creates thick film as it dries locally
- Did not yield low adhesion in wet state

Solid friction modifier

- Same amount-to-CoF dependency as liquid TOR/FM
- In field, overapplication should be hard to reach

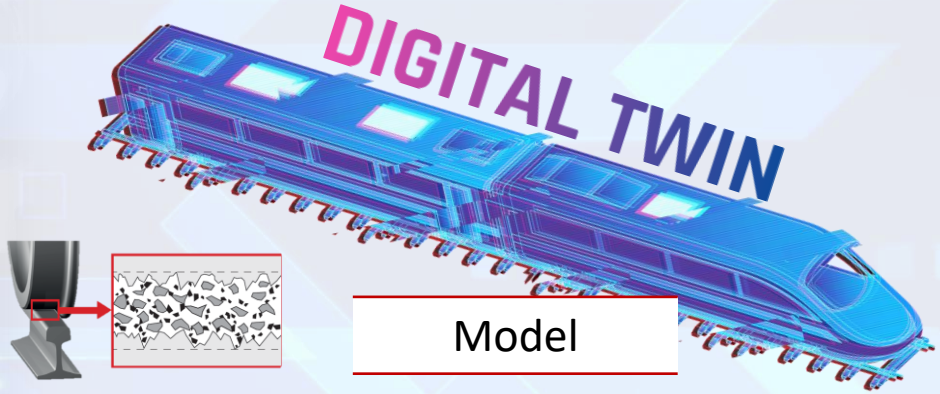

Model

- Replicates EHL to BL transition with TOR

However

- Dependent on correct film prediction
- Asperity distribution can be non-Gaussian
- Different models for elasto-plastically deforming asperities

What's next ?

Transient adhesion effects

Using results for real wheel-rail contact

NOVELTY

Development of a frictional model considering asperity contact and lubrication regime.

New knowledge on conditions that could lead to low adhesion with TOR products.

Describing influence of TOR lubricant solid particle in relationship to low adhesion conditions.

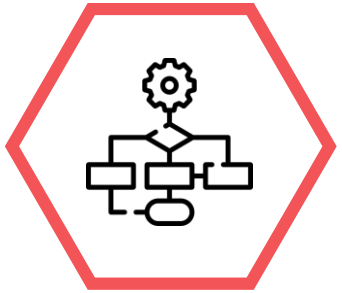

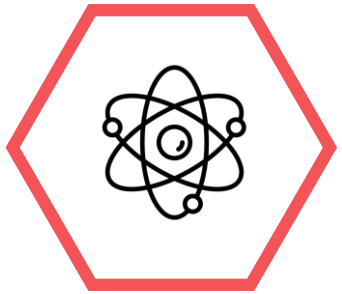

PRACTICAL APPLICATION

Use for a digital twin in combination with top of rail friction management in wheel-rail contact.

Identifying frictional inputs for dynamic simulations considering top of rail friction management.

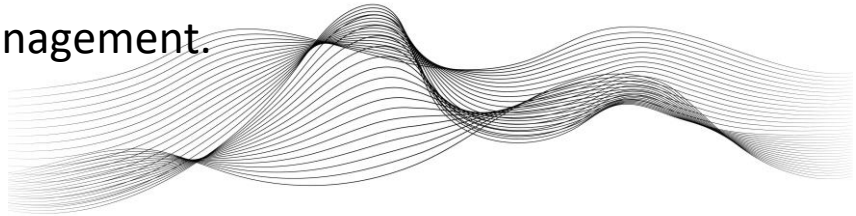

Application to other areas such as flange lubrication, rain influence and general contamination of wheel-rail interface.

LIST OF PUBLICATIONS

KVARDA, D., R. GALAS, M. OMASTA, L.B. SHI, H.H. DING, W.J. WANG, I. KRUPKA and M. HARTL. Asperity-based model for prediction of traction in water-contaminated wheel-rail contact. *Tribology International*, 2021, 157, 1–11. **(JIF 6.2)**

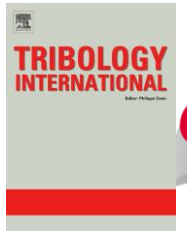

KVARDA, D., S. SKURKA, R. GALAS, M. OMASTA, L.B. SHI, H.H. DING, W.J. WANG, I. KRUPKA and M. HARTL. The effect of top of rail lubricant composition on adhesion and rheological behaviour. *Engineering Science and Technology, an International Journal*. 2022, 35, 1–9. **(JIF 5.7)**

KVARDA, D., R. GALAS, M. OMASTA, M. DZIMKO, I. KRUPKA and M. HARTL. Shear properties of top-of-rail products in numerical modelling. *Proceedings of the Institution of Mechanical Engineers, Part F: Journal of Rail and Rapid Transit.* 2022, 0, 1–10. **(JIF 2.0)**

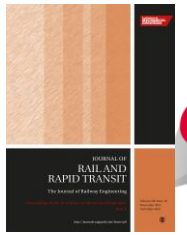

LIST OF PUBLICATIONS - OTHER

GALAS, R., D. KVARDA, M. OMASTA, I. KRUPKA and M. HARTL. The role of constituents contained in water–based friction modifiers for top–of–rail application. *Tribology International*. 2018, 117, 87–97. **(IF 5.620)**

SHI, L.B., Q. LI, D. KVARDA, R. GALAS, M. OMASTA, W.J. WANG, J. GUO and Q.Y. LIU. Study on the wheel/rail adhesion restoration and damage evolution in the single application of alumina particles. *Wear*. 2019, 426-427, 1807–1819. **(IF 4.695)**

SHI, L.B., C. WANG, H.H. DING, D. KVARDA, R. GALAS, M. OMASTA, W.J. WANG, Q.Y. LIU and M. HARTL. Laboratory investigation on the particle-size effects in railway sanding: Comparisons between standard sand and its micro fragments. *Tribology International*. 2020, 146, 1–12. **(IF 5.620)**

REMESOVA, M., S. TKACHENKO, D. KVARDA, I. ROCNAKOVA, B. GOLLAS, M. MENELAOU, L. CELKO and J. KAISER. Effects of anodizing conditions and the addition of Al2O3/PTFE particles on the microstructure and the mechanical properties of porous anodic coatings on the AA1050 aluminium alloy. *Applied Surface Science.* 2020, 513, 1–10. **(IF 7.392)**

LI, Q., B.N. WU, H.H DING, R. GALAS, D. KVARDA, Q.Y. LIU, Z.R. ZHOU, M. OMASTA and W.J. WANG. Numerical prediction on the effect of friction modifiers on adhesion behaviours in the wheel-rail starved EHL contact. *Tribology International*. 2022, 170, 1–11. **(IF 5.620)**

NAVRATIL, V., R. GALAS, M. KLAPKA, D. KVARDA, M. OMASTA, L.B. SHI, H.H. DING, W.J. WANG, I. KRUPKA and M. HARTL. Wheel squeal noise in rail transport: the effect of friction modifier composition. *Tribology in Industry.* 2022, 44, 361–373.

LI, Q., S.Y. ZHANG, B.N. WU, Q. LIN, H.H DING, R. GALAS, D. KVARDA, M. OMASTA, W.J. WANG and Z.F. Wen. Analysis on the effect of starved elastohydrodynamic lubrication on the adhesion behavior and fatigue index of wheel-rail contact. *Wear*. 2022, 510-511, 1–12. **(IF 4.695)**

Thank you for your attention !